# Design and test of a heat pipe for geothermal applications

Paul-Jan Hogendoorn

**Department document number:**
2990

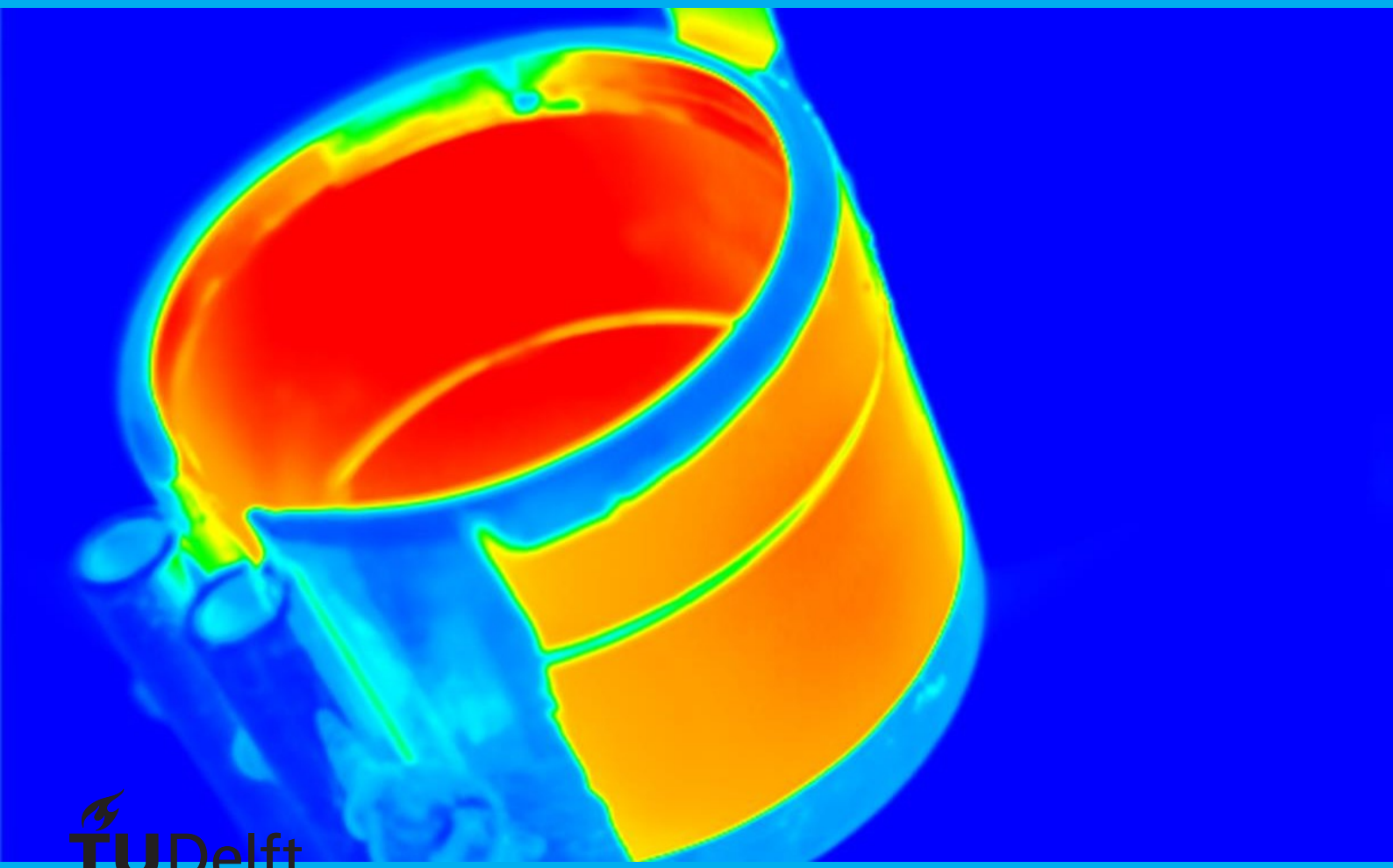

TU Delft

# Design and test of a heat pipe for geothermal applications

by

Paul-Jan Hogendoorn

to obtain the degree of Master of Science
at the Delft University of Technology,
to be defended publicly on Tuesday September 10, 2019 at 9:30 AM.

| | | |
|---|---|---|
| Student number: | 4304179 | |
| Project duration: | September 14, 2018 – September 10, 2019 | |
| Thesis committee: | Prof. dr. ir. B. J. Boersma, | TU Delft, supervisor |
| | Dr. R. Delfos, | TU Delft, supervisor |
| | Dr. Ir. M. J. Tummers, | TU Delft |
| | Ir. A. Twerda, | TNO |

An electronic version of this thesis is available at `http://repository.tudelft.nl/`.

TU Delft

# Abstract

Heat pipes are typically used in the semiconductor industry. This means that the scale of these heat pipes is typically in the order of centimeters. Zijm [27] suggests that heat pipes could be used for geothermal applications, but literature is lacking. To further investigate the geothermal application of heat pipes, a large scale heat pipe is built. This thesis gives an insight in the typical design challenges that one faces when constructing a heat pipe of this scale. The heat pipe that is constructed can support a heat flow of 10 kW. The heat pipe is constructed from mainly 54 millimeter copper and glass pipes. The evaporator section is 1.5 meters long and facilitates controlled electric heating. Then follows a 4 meter long adiabatic section. The condenser section is 2.5 meters long. The total length of the heat pipe is 9 meters. The individual sections are held together by EPDM connectors. The dimensions of the heat pipe are compared to the operational limits posed by the Engineering Sciences Data Unit [3]. Then the thermal resistances of the heat pipe sections are calculated and afterwards validated. The interfacial thermal resistance between the electric heaters and evaporator wall was reduced by applying thermal conduction paste to the band heaters. It was found that at coolant flows of 1000 l/h and higher, the vapour temperature in the heat pipe drops significantly. The drop in temperature facilitates a higher heat flow through the heat pipe. Also, the resistance across the evaporator and the condenser section gets smaller for higher coolant flows. The results found are supported by theory and formulae from the Engineering Sciences Data Unit.

# Acknowledgements

For the past months I have been busy with building a heatpipe. I had a blast doing it, but I could not have done it without the help of so many people. I want to dedicate this page to all those wonderful people that made this project what it is.

First, a big 'thank you' to my supervisors. By helping me and being critical, they shaped the heat pipe the way it is. René, you were very helpful with your remarks and time. Bendiks, your help was always practical and if I had any engineering problem, you were happy to help. Also Bart Hoek, you saw a lot of bumps on the road, but by being critical you helped me think about things I would not have considered otherwise. Thank you for the support and the liters of coffee and tea that I could consume by using your coffee pass.

Also, Jaap van Raamt thank you for keeping up with the constant stream of questions and (cancelled) orders. You were extremely helpful and a always kept calm. Daniël, thank you for all the time you invested in my project. Just do not drive over my copper pipes again. However, you more than made up for it by all the time and attention you gave to the soldering of the parts. Also, Jasper thank you for turning the brass parts on your lathe. You did an outstanding job and made the project so much easier on my mind. Last but certainly not least: Martijn, thank you for your time. You made the project so much better, without your knowledge of the electric parts I would not have been able to do it.

Finally, thanks to my parents who supported me through this project. A lot of evenings I came home late because of philosophy classes or because I had to finish certain things in the lab. Thank you for keeping the food warm and being so patient.

*Paul-Jan Hogendoorn*
*Delft, August 2019*

# Contents

# 1 Introduction

In 2017, the Netherlands used a total 3156 PJ of energy [24]. About 716 PJ is lost by transportation and other losses, which leaves 2440 PJ that can be used by the end user. From that 2440 PJ, 41% is used for heating. That is 1000 PJ of energy used purely to heat homes, cook etc. To put these numbers into perspective: with one petajoule of electrical energy, one can drive around the world 42 thousand times in a Tesla Model 3 (with a power consumption of 0.16 kWh/km). One petajoule is equivalent to the total energy output of 96 of the biggest windmills on earth (Haliade-X 12MW) turning at full capacity for one day.

By creating alternative sources for heating, we can reduce the need for fossil fuels that are now used for heating. The majority of this heat comes from fossil resources (mainly natural gas). If this heat can be extracted elsewhere, the Netherlands could save a significant portion of its fossil fuel use. P. Zijm [27] suggests in his work to extract geothermal energy from the earth, by employing abandoned oil and gas boreholes. These holes can be up to 2 kilometers deep [14]. At these depths, typical temperatures that are encountered are in the order of 90 $^{o}$C [21]. Zijm warns that open systems (systems that pump hot groundwater to the surface and use it without returning water to the ground) deplete groundwater sources. To overcome this problem, a closed system is suggested, so that no groundwater is pumped to the earth's surface. To extract heat without significant energy losses for pumping, Zijm suggests the use of heat pipes. Heat pipes are generally used for cooling in the semiconductor industry. The length of those heat pipes is typically in the order of centimeters. Larger heat pipes can be found in vacuum tube solar boilers, where lengths go up to meter scale. To use heat pipes for geothermal applications, more research is needed for scaled up heat pipes. This thesis investigates the design process of large-scale heat pipes. The goal of this project is to build a large-scale heat pipe setup to further investigate the dominant large-scale effects in heat pipes.

## 1.1. Heat pipes

The first patent for a working heat pipe was filed by Gaugler [9]. In this patent he describes the basic working of a heat pipe. The advantage of using a heat pipe is that it can transfer heat over distances without a the need for a significant temperature gradient. Theoretically, the pressure in a heat pipe can be tuned to the temperature at which the heat source delivers its heat. A heat pipe in its most basic form is a closed tube that contains a working fluid. This working fluid is evaporated in a heater section as can be seen in figure 1.1. Here heat enters the heat pipe. The heat is absorbed by the working fluid which then evaporates. The vapour goes up into the heat pipe. The vapour flows first through the adiabatic section which keeps the vapour at constant temperature and pressure. When it comes to the top, there is a condenser section that extracts heat from the heat pipe. The working fluid then condenses at the wall of the condenser. This fluid flows down along the wall under the influence of gravity. The fluid goes down to the evaporator of the pipe, where it can be boiled again and the process will start over. The way in which the heat pipe redistributes its liquid varies. In the original patent of Gaugler, he describes a 'porous capillary structure' [9]. The porous material can distribute the condensed working fluid, using capillary action. Later on, other ways of distributing the working fluid were found. ESDU recognizes four different heat pipes [2]: capillary-driven, flat-plate heat pipe, two-phase closed thermosypon and a rotating heat pipe. The capillary-driven heat pipe is described by Gaugler. The flat-plate heat pipe has a horizontal orientation. The working fluid distributes itself, using gravity, along the

bottom evaporator plate. However, sometimes a wick (a finely woven mesh of metal wires) is used to distribute the liquid more efficiently. Flat-plate heat pipes have a distinctive small aspect ratio. A rotating heat pipe distributes its liquid using centrifugal forces. These heat pipes have a tapered wall and under rotational velocity, the liquid working fluid is forced back to the evaporator. The two-phase closed thermosyphon has been described above. Not a wick is used to get the condensed working fluid back to the evaporator, but gravity. In two-phase closed thermosyphons, the condenser is typically situated above the evaporator, to ensure that the working fluid flows back. For more information on the differences between the heat pipes, please refer to this ESDU paper [2]. In this thesis, the terms (two-phase closed) thermosypon and heat pipe are used interchangeably, since this report mainly deals with the two-phase closed thermosypon.

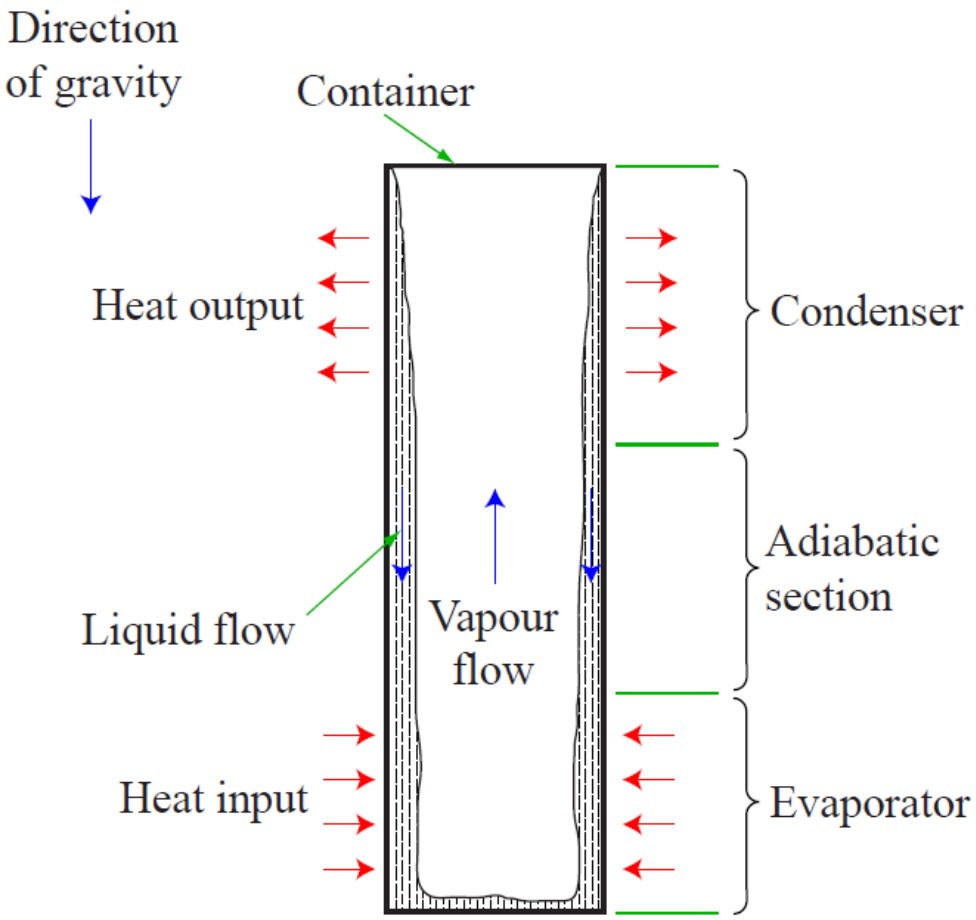


Figure 1.1: Schematic overview of a heat pipe [2]

The innovation of heat pipes is that one can transfer heat efficiently from one place to another because the heat is stored in a phase change (i.e. latent heat) of working fluid. This means that the heat that is put in at the evaporator side can be almost completely recovered, resulting in a very efficient process. The phase change takes place under constant temperature. Hence, only a small temperature difference is needed between the heat source and the heat pipe.

To illustrate the difference between pure conduction and using a heat pipe to transfer heat let us take the following example: say one wants to transfer 10 kW of heat over a distance of 10 meters. To minimize the resistance, one chooses a block of solid copper of 1x1x10 meters. Using Fourier's law of thermal conduction [15]:

$$\frac{\dot{Q}}{A} = -k\frac{dT}{dx} \tag{1.1}$$

With $\dot{Q}$ being the heat transfer rate, $A$ the cross-sectional area, $k$ the thermal conductivity and $\frac{dT}{dx}$ the change in temperature in x-direction. We assume that temperature is linearly dependent on x, and that the thermal conductivity is constant. For copper, $k$ is around 400 $W/(mK)$ and the cross-sectional area is 1 $m^2$. The distance over which we want to transfer heat is 10 meters. The heat transfer rate is 10 kW. Rewriting equation 1.1 and isolating $dT$ gives:

$$\Delta T = \frac{\dot{Q}\Delta x}{-Ak} = \frac{10000 \cdot 10}{1 \cdot 400} = 250^o C \tag{1.2}$$

250 $^oC$ is an order of magnitude bigger when we compare it to the temperature difference that is needed for a heat pipe (we will discuss this is in chapter 2). For heat pipes, the only thermal resistance that needs to be overcome is in the walls of the heat pipe. This is why heat pipes can operate while maintaining a low temperature gradient.

## 1.2. Structure

The thesis is divided into three chapters. The second chapter of this thesis will give an overview of the theoretical background of heat pipes and the design considerations. Here one can find the calculations for the dimensions of the heat pipe and why certain materials were chosen. Also various drawings and photo of the heat pipe are discussed. The third chapter will cover the results of the measurements and an interpretation of the results is given. The fourth chapter discusses the results and gives recommendations for further research.

# 2

# Design

Before the heat pipe was built, there were some requirements discussed:

1. The energy throughput should be in the order of 10 kilowatt, in order to have a high heat transfer but stay below the theoretical limits as discussed in paragraph 2.5.
2. Some parts must be transparent in order to be able to observe the liquid film, the evaporation and the condensing process.
3. The height of the heat pipe should as large as reasonably fitting in the laboratory, in order to study the hydrostatic forces that are relevant for the application.
4. The operating temperature should be in the range of 50 to 80 $^{o}$C, which is a typical temperature range for geothermal applications.
5. Use materials that are durable and can withstand temperatures of around 100 $^{o}$C, so it can endure the operating temperature.

## 2.1. Dimensioning the heat pipe

The height of the heat pipe is restricted by the height of the lab hall of the Process & Energy Department. The frame that supports the heat pipe, is 12 meters high. Given that there needs to be space under the heat pipe for the placement of a high speed camera and the fact that the pipe needs to be manually and optically accessible from the top, restricts the total length of the heat pipe to 9 meters.

The choice for the diameter of the pipe was restricted by the available dimensions of so-called band heaters. Band heaters as a heat input on the evaporator side are preferred because of the high temperatures they can withstand and the high power density they provide in a controlled way. A second consideration is the standard available diameters of copper piping. Copper is preferred because of its high thermal conductivity while having a relative high yield strength. Standard diameters for copper tubes (made by KME Sanco) are 42, 54, 64 or 76.1 millimeters [10]. This gives a diameter range in which one can search for a suitable heater. Now the band heater with the highest power density is chosen, which has an internal diameter of 51 millimeter. The band heater manufacturer offers an option to slightly open the band heaters, which makes it fit the 54 millimeter copper pipe. Therefore, the diameter chosen of the copper pipe is 54 millimeter.

## 2.2. Sensor placement

Based on Zijm's work [27] and based on the requirements mentioned above, a Piping and Instrumentation Diagram (P&ID) is made to visualize the different components needed and their position. The setup is similar to Zijm's setup, but there are some key differences: the number of heaters used (indicated in figure 2.1 as HE: Heating Element) are 8 instead of 2. Since one individual heater can provide 1200 watt, 8 are needed to give 9600 watt. On the heaters, thermocouples are placed to monitor the temperatures of the heaters (indicted

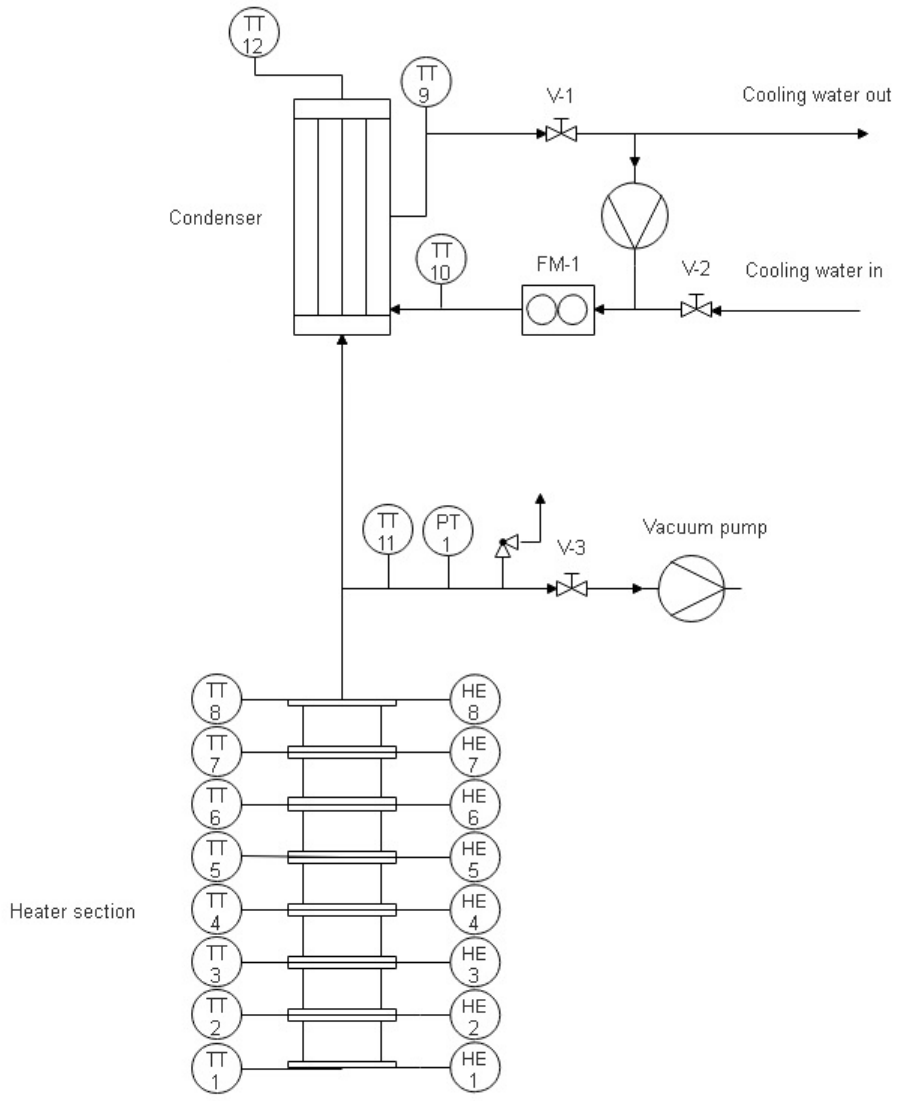


Figure 2.1: Piping and Instrumentation Diagram of the heat pipe

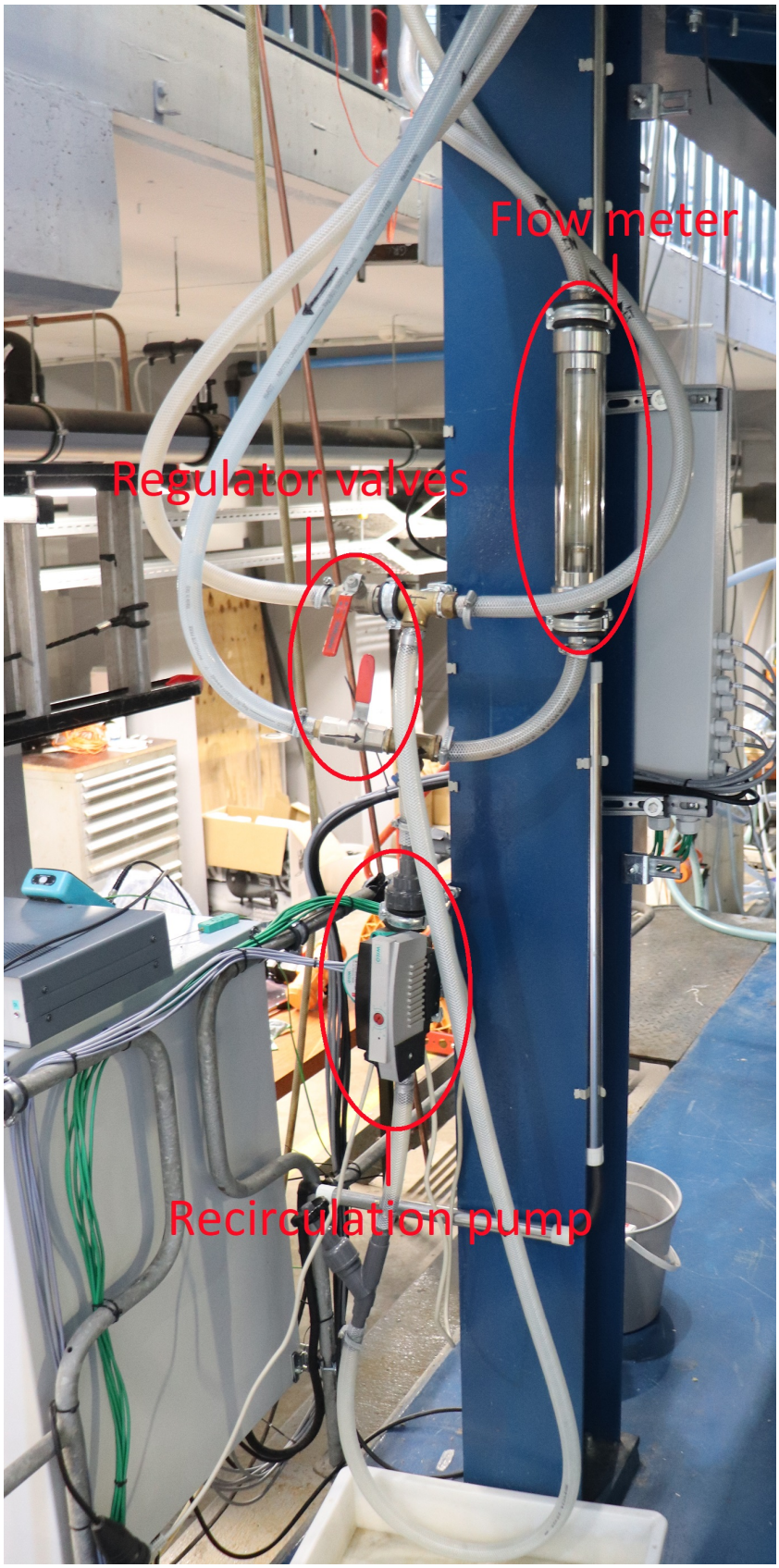


Figure 2.2: Picture of the coolant flow controls.

by TT: Temperature Transmitter). The construction directly above the heater section is based on Zijm's idea; only a safety valve is added to make sure that the construction can not explode in case that the pressure and temperature rise too high. Zijm made a smaller diameter take-off branch into his setup onto which he could attach any desired sensor, because it is almost impossible to directly insert sensors into a 54 mm pipe. In the take-off branch, a pressure sensor (indicated by PT: Pressure Transmitter) is mounted to monitor the pressure in the heat pipe. Using the pressure sensor information, one can determine if the vapour is saturated and if there is air leaking into the setup. On the end of the branch a regular gas valve is mounted to seal off the tube that goes to the vacuum pump. If it turns out that air is leaking into the heat pipe, the vacuum pump can be used to lower the pressure in the heat pipe. The condenser section of the pipe is a double walled tube. Zijm encountered numerous problems because he used a plate heat exchanger. Due to air leakage, the plate heat exchanger got obstructed by stagnant air, which made the flow of condensed water back into the heat pipe impossible. To combat this problem, a double walled tube is used, since this tube will not get obstructed as easily. To monitor the heat flow out of the condenser, two PT-100 sensors are mounted on the in- and outlet wall of the condenser. Since the wall is made from copper, the thermal resistance across the wall is negligible. PT-100 sensors are preferred over thermocouples because of their accuracy and because they are not as sensitive to noise. Beside the PT-100 sensors, a flow meter (indicated by FM: Flow Meter) is used to monitor the volumetric flow of coolant. Having the mass flow and the in- and outlet temperature of the condenser gives the user information about the heat flow (since $\dot{Q} = \dot{m}c_p\Delta T$). To give the user more control over the heat pipe, a re-circulation line is added to give control over the inlet temperature of the condenser. Also, the condenser has been over-dimensioned so the temperature in the heat pipe can be controlled by the coolant flow. In figure 2.2 one can see the devices that are implemented in the cooling circuit. On top of the condenser, a PT-100 is mounted in order to measure the thermal losses of the heat pipe. It is also an indication if the heat pipe is working properly; to check if the vapour is reaching the top of the condenser.

## 2.3. Material selection and design

Since the copper tubes that are being used are only available in lengths of 5 meters, it is decided to build the adiabatic section of the heat pipe with the leftover copper from the evaporator and the condenser section. To make certain parts of the heat pipe transparent, a different material is needed. PMMA and polycarbonate are considered, but they are prone to deformation when exposed to temperatures higher than 50 $^{o}$C (see figure 13.7 in Ashby [5]). Soda-lime glass has relatively high thermal expansion coefficient, which makes it unfit to resist thermal shock (figure 12.4, Ashby). Therefore, borosilicate glass is chosen for its high melting point and

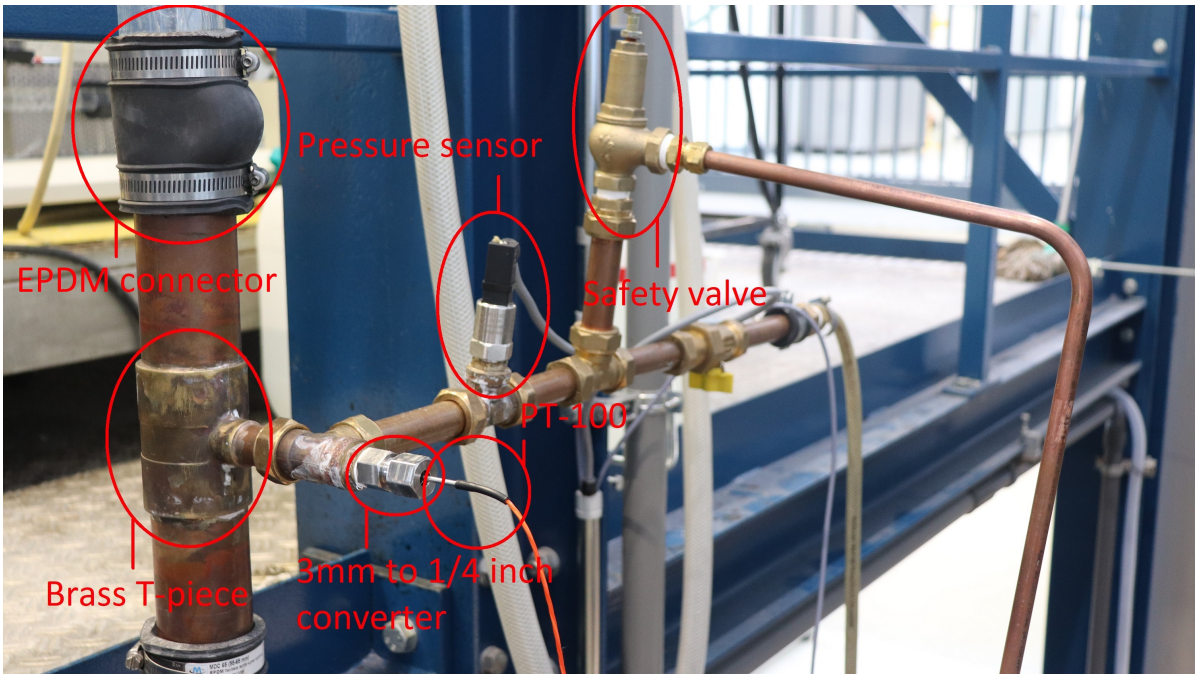


Figure 2.3: Picture of the brass T-piece and the sensors it facilitates.

resistance against creep, even for prolonged periods of thermal stress.

### 2.3.1. Connector choice

To connect the glass to copper piping, a tube connector made from EPDM was used. EPDM is a rubber-like material that can easily withstand temperatures up to 130 $^{o}$C while it does not degrade when it comes in contact with steam (in contrast to Viton). Also, it is a high-density material which makes it fit for vacuum conditions. The tube connectors are readily available at any DIY store.

To insert measurement devices into the heat pipe, brass T-pieces are used. They are soldered into the heat pipe with a 22 mm copper pipe branching out. Onto this 22 mm pipe, any standard 22 mm compression fitting can be attached. The outgoing 22 mm pipe is slightly angled, to ensure that condensed vapour will flow out, into the setup. Figure 2.3 shows the T-piece with the connectors and sensors that are attached.

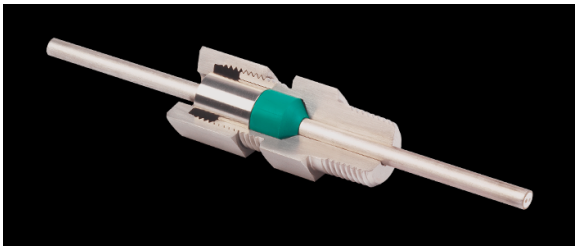

Figure 2.4: 3mm to 1/4 inch thread converter [7]

To convert a 22 mm pipe to a 3 mm PT-100 sheath, one can use a different kind of pressure fitting as shown in figure 2.4. In the centre of the fitting a 3 mm pipe is set. Around the 3 mm pipe, a Viton ring is shown (the green ring in the figure). This ring is put into a tapered hole. On top of the ring a metal part is made. This metal ring pushes the Viton ring into the tapered hole, thereby securing the 3 mm pipe into its place.

To connect cooling water to the setup, flexible PVC hoses are preferred. The flexible hoses can be bent and offer more degrees of freedom than rigid piping. Since the inside diameter of the copper pipes is 20 mm, the flexible hoses are also chosen to be 20 mm. To connect the hoses to the pipe, brass hose tails are used. These fittings have on one side multiple wedge-like shapes to hold the hose in place. Over the flexible hose, a pipe clamp is fitted to secure the hose to the hose tail. On the other side of the hose tail, standard 3/4 inch thread is used. These thread onto 22mm pressure fittings, as can be seen in figure 2.5.

Figure 2.5: Picture of a brass hose tail and the flexible PVC hoses.

### 2.3.2. End caps

To seal off the ends of the heat pipe, a removable construction is needed that is both air and water tight. Besides, it should be transparent so one can observe what happens in the evaporator and condenser section. A construction is made as shown in figure 2.6. On the top of the figure, the copper tube is shown at the end of which a brass flange is soldered. Brass is chosen because it can be easily machined and it can be soldered onto copper. On the copper flange a glass holder is fastened. The glass holder is made from aluminum, because of its corrosion resistance (table 17.3 Ashby [5]). Water and especially steam condensate is highly corrosive. In the glass holder, a small glass window is installed. The glass is held in place by an aluminum ring that can be fastened to both the glass holder and the brass flange. The whole construction is tightened together with M5 bolts and nuts. In the glass holder, 2 grooves are made in which O-rings are laid. The rings are also made from EPDM. For a detailed, technical drawing of the glass holder, please refer to Appendix A.1.

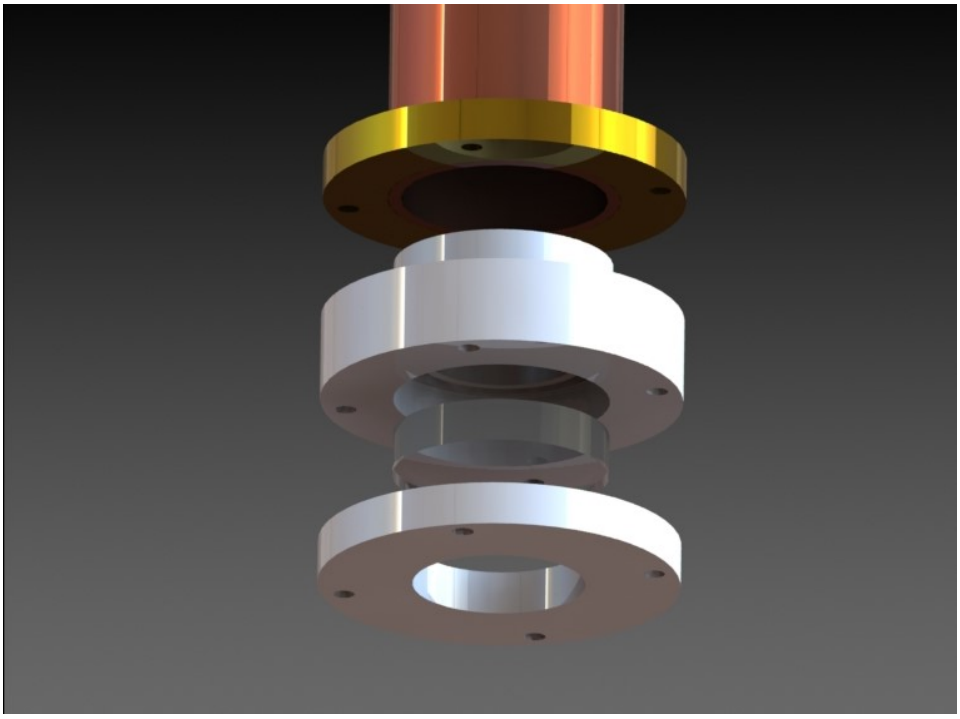

Figure 2.6: Exploded view of the assembly that seals the ends of the copper tube

Figure 2.7: A cross-sectional view of a model condenser

### 2.3.3. Condenser section

In figure 2.7, one can see a cross-section of the condenser. The condenser section is a double walled tube. In between the two walls, water can flow, to cool the setup down. The condenser is hand made. The outside wall is made from 64 mm copper tube with a 2 mm wall thickness and the inside wall from 54 mm tube; leaving a gap of 3 mm in between the pipes (since (64-2•2-54)/2=3). The two pieces of copper are connected to each other using brass flanges. In the 64 mm tube, two 22 mm holes are drilled to connect it to cooling water. In the two holes, 22 mm copper pipe is soldered which in turn is connected to flexible PVC tubes that go to the in- and outlet of the cooling water. After construction, the pipe is insulated to make sure that the environment will not influence the temperature of the coolant.

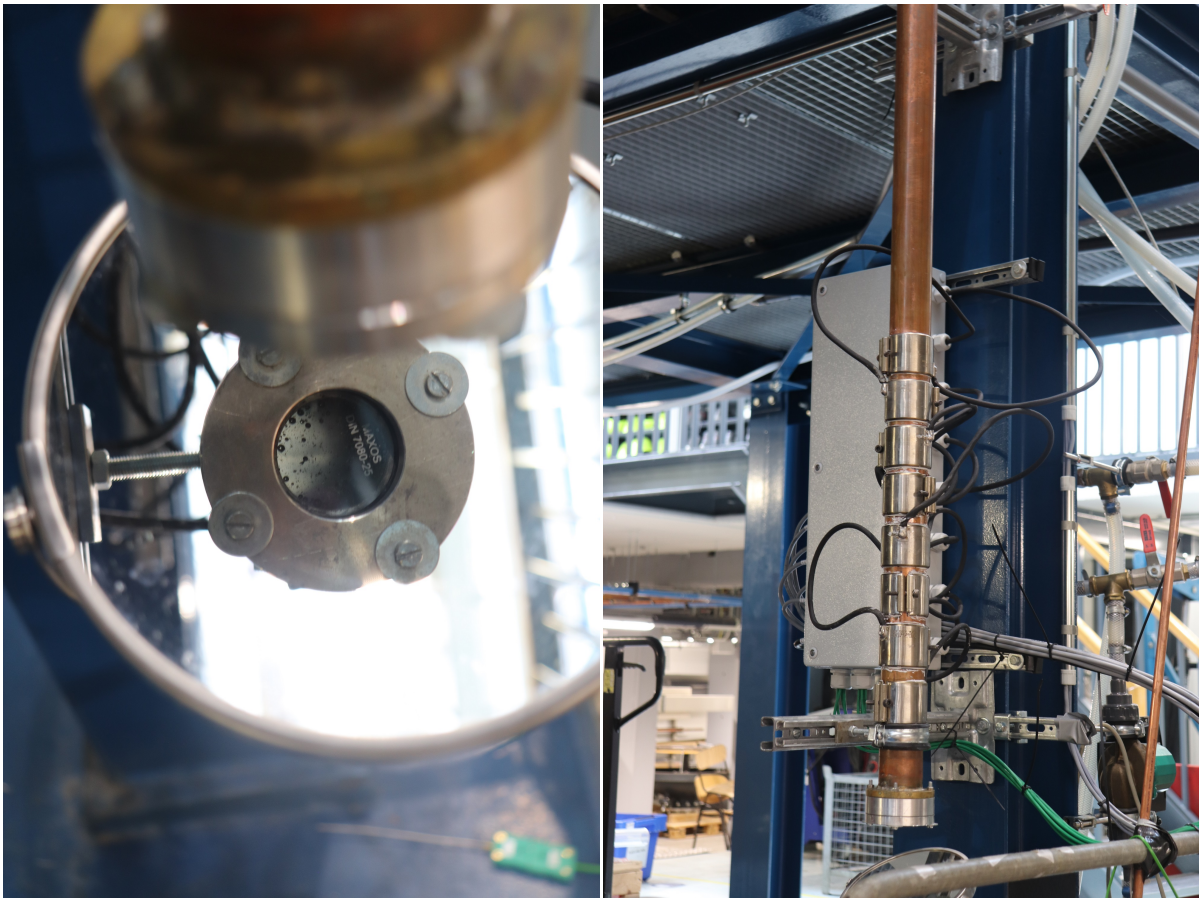

(a) The evaporator section seen from below.

(b) The evaporator section with its band heaters.

Figure 2.8: The evaporator section seen from the side and below.

### 2.3.4. Evaporator section

The evaporator section is constructed from a piece of 54 mm copper pipe. On the outside of the pipe, 8 band heaters are placed. The total length of the boiler section is 1.5 meter. This length is chosen to add more band heaters in the future when required, or to add more space in between the band heaters. Currently the band heaters are all stacked on the bottom of the evaporator. The evaporator is located directly below the brass T-piece that has been explained in paragraph 2.3.1. The evaporator is connected to the T-piece with an EPDM tube connector. It was decided to not make a rigid, non-removable connection to the T-piece because this would make it impossible to remove or add band heaters to the boiler section.

### 2.3.5. Insulation material

Three different materials are considered for the insulation of the heat pipe: Rockwool, Armaflex and vermiculite. Vermiculite is a commercial insulation product made from a mineral. It can handle high service temperatures. Compared to the other insulation products, it is a dense and heavy material. The problem that arises from this property is that vermiculite has a much higher heat capacity than the other products. This makes that the reaction time of the heat pipe to thermal changes, will be longer. Since better options are available, vermiculite is not considered any further. The second insulation material considered is Armaflex. This is a thick foam product. It has a low density and is flexible. Its maximum service temperature is around 100 $^{o}$C, which makes it unfit to insulate the band heaters, since the band heaters can achieve much higher temperatures, as we will see in chapter 3. The third product considered is Rockwool, which is a stone wool. It has high service temperatures, has a low density and is sold with a pre-installed, aluminum heat shield. It is not as flexible as Armaflex, but is offered in a range of different thicknesses. To make an objective comparison, the performance of Rockwool and Armaflex are calculated. To study their performance a case study is made. Take a 10 meter long copper pipe with a 54 mm diameter and with a liquid inside that has a tem-

perature of 50 $^{o}$C. The conduction coefficient of both Armaflex and Rockwool is taken as 0.04 W/mK (which is a typical value for stagnant air [8]). The convection coefficient on the outside of the heat pipe is taken as 5 W/m$^2$K. Since the pipe is made from copper, the resistance across the copper pipe wall is not considered. The emissivity from the outside wall of Rockwool is taken as 0.1, while the emissivity of Armaflex is 0.9 (Table A.5 Mills [15]). To calculate the emissive losses from the surface of the Armaflex and Rockwool, we can use the following linearization [15]:

$$h_r = 4\epsilon\sigma T_w^3 \tag{2.1}$$

Where $h_r$ is the radiation heat transfer coefficient, $\epsilon$ is the emissivity of the material, $\sigma$ the Stefan-Boltzmann constant ($5.67 \bullet 10^{-8}$) and $T_w$ is the temperature of the outside surface of the insulation material. The surface temperature of the insulation material is initially unknown. To calculate the surface temperature, we can iterate by first guessing the surface temperature and afterwards calculating the temperature. This value can then be fed back into the equations.

Armaflex comes in one size, which has a wall thickness of 13 millimeters. Rockwool shells come in three different wall thicknesses: 25, 30 and 40 millimeters. To calculate the resistance across the shell, we use from Mills:

$$z = \frac{\ln(R_o/R_i)}{2\pi k l}$$

Where $z$ is the thermal resistance across the insulation shells, $R_o$ is the outside radius, $R_i$ is the inside radius of the insulation and $l$ is the length of the copper pipe. Now that the resistance is known we can fill in:

$$\frac{1}{U} = \frac{1}{(h_r + h_c)A_{im}} + \frac{1}{z}$$

Where $\frac{1}{U}$ is the overall resistance of the insulation shells, $h_c$ is the convective heat transfer coefficient and $A_{im}$ is the outside area of the insulation material. Since the Armaflex has a smaller radius, the area over which it can lose becomes smaller as well. To calculate the heat loss through the insulation we use:

$$\dot{Q} = U * (T_w - T_e) \tag{2.2}$$

Now that the total heat flow is known, we can calculate the temperature of the wall for this heat flow. Using that:

$$\Delta T = \dot{Q} \bullet z$$

Where $\Delta T$ is defined as the temperature difference between the inside wall of the insulation material and the outside wall temperature. Iterating this process to get the wall temperature to a satisfactory value, gives that the heat loss for Armaflex is 154 watt. For the Rockwool it is 95, 86 and 74 watt for the wall thicknesses 25, 30 and 40 millimeter respectively. From these calculations it becomes clear that Rockwool is the superior product. To minimise losses, the thickest shell is chosen.

| **Brand** | **Wall thickness [mm]** | **Outer diameter [mm]** | **Heat loss [W]** |
|---|---|---|---|
| Rockwool | 25 | 104 | 95 |
| | 30 | 114 | 86 |
| | 40 | 134 | 74 |
| Armaflex | 13 | 80 | 154 |

Table 2.1: Overview of the thermal losses for the various insulation materials

### 2.3.6. Heat pipe fastening to frame

To suspend the heat pipe, a construction is made from Flamco brackets [23], as can be seen in figure 2.9. The clamps around the heat pipe are standard Flamco clamps. The clamps have a rubber ring inside, to thermally insulate the heat pipe from the steel clamp and give a better grip. The clamps have M8 thread to which one can attach stud bolts. The stud bolts can be any desired length. The stud bolts are attached to a bracket to support the weight. The bracket is bolted to a standard Flamco rail. In total 11 of these assemblies are used to suspend the heat pipe.

Figure 2.9: Clamping system to fasten the heat pipe to a frame.

### 2.3.7. Electrical setup

Essential to the functioning of the heat pipe is the electrical setup for the heat pipe. What the setup looks like can be found in figure 2.10. In figure 2.10a one can see the front panel of the system. On the left 2 switches are found that turn the water and vacuum pump on and off. Below the switch, a reset button can be found, which can reset the setup. In the middle there is an emergency stop button for if anything goes wrong. Next to the emergency stop, a temperature controller is situated. This controller is the RKC MA-901 controller (8 channel version) [11]. This controller gets a thermocouple reading and from this value it outputs a signal that goes to the solid state relays (figure 2.10b). The thermocouple reading comes from the band heaters. On the outside of the band heaters, a thermocouple is located that indicates what the temperature of the band heater is. This temperature is fed to the temperature controller which feeds the value into a PID controller. The values of the PID controller are all manually tuned, to smoothen the output signal to the solid state relays. On the front panel of the temperature controller, one can give in a desired temperature of the band heaters and the temperature controller will signal to the solid state relays how much electrical power must be let through to the band heaters in order to obtain the set temperature. The solid state relays can switch on or off at the zero crossing of any AC signal. In the case of this setup, the AC signal is grid power. Since the solid state relays can switch twice for every period, the relays can switch a hundred times per second for a 50 Hz signal. This electrical power is then sent to the band heaters, that converts the electrical power into heat. On the right of the temperature controller, a pressure read-out can be found. This panel gives an indication of what the relative pressure is in the heat pipe. Because it is only an indication, it has not been calibrated to the pressure sensor. The signal that the pressure sensor gives out is split into two. One goes to the pressure read-out panel, the other to the RS-485 converter. This converter converts the output signal of the pressure sensor (a 4-20 mA signal) into a digital signal (RS-485). The RS-485 converter does not only convert the signal from the pressure sensor. It also converts the signal from the PT-100 temperature sensors. The RS-485 converter sends its signal to the computer, which reads the signal and puts it into a graph. The software used on the computer is Specview [13]. Specview logs the values and can export them into a CSV-file for further data analysis.

## 2.4. Working fluid selection

An important parameter for the workings of a heat pipe is its working fluid. For wicked heat pipes (i.e. heat pipes that contain a wick to transport fluid), the heat flow is limited by the capillary capacity of the wick. This limit is reached when the capillary 'pumping' pressure is equal to the pressure losses in the pipe:

$$\Delta P_{cap} = \Delta P_{liq} + \Delta P_{vap} + \Delta P_{grav}$$

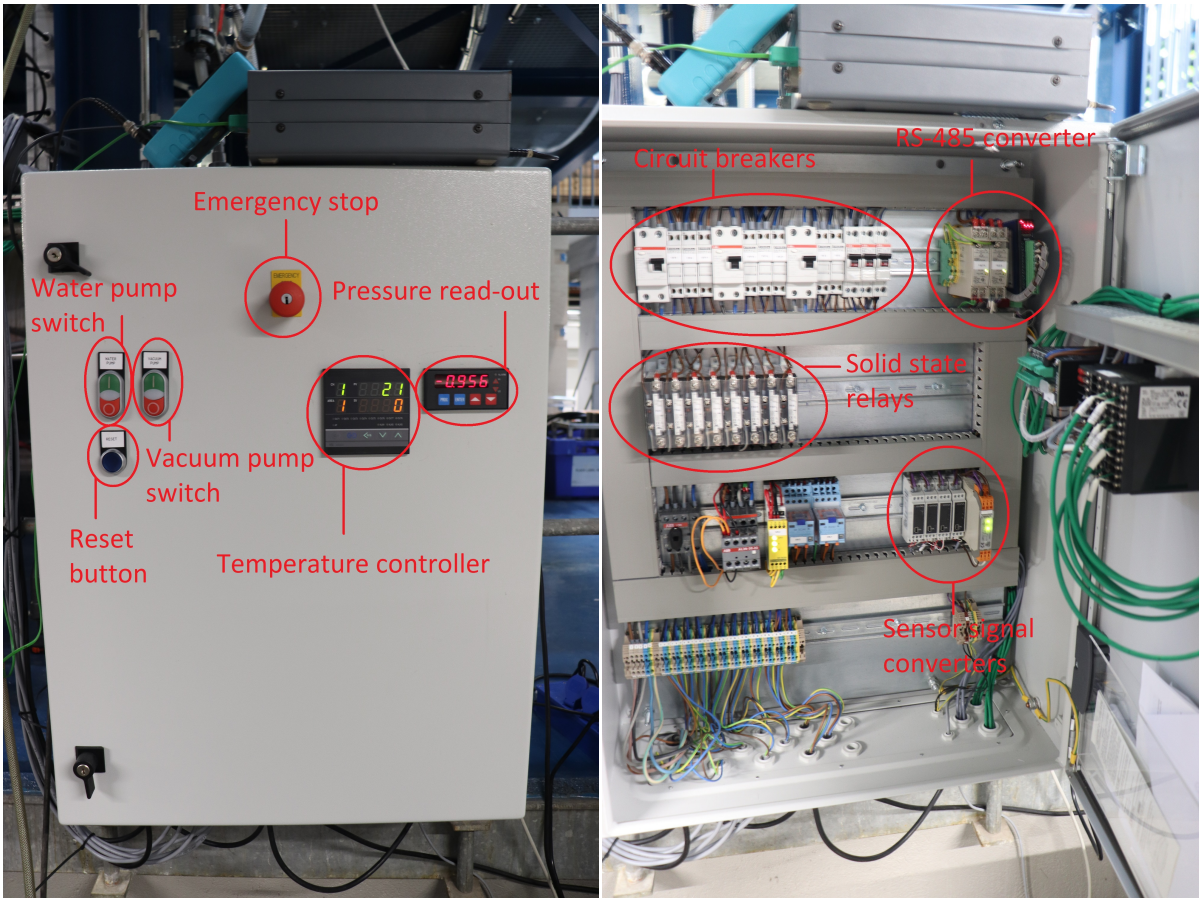


(a) The front pane of the box that houses the electric components.

(b) Inside of the box that houses the electric components. Important components have been named.

Figure 2.10: View of inside and outside of the electric control box.

Where $\Delta P_{cap}$ is the capillary pressure, $\Delta P_{liq}$ pressure losses due to the liquid going through the wick, $\Delta P_{vap}$ vapour pressure losses due to vapour flowing through the heat pipe and $\Delta P_{grav}$ accounts for the hydrostatic pressure. Given that there are no gravitational losses and no vapour losses (or they are an order of magnitude smaller compared to the liquid pressure loss), the only loss that is considered is the liquid pressure loss. Hence, the capillary pressure ($\Delta P_{cap}$) should be equal to $\Delta P_{liq}$. For a wicked heat pipe, one can choose a working fluid using a Figure of Merit (FoM). Using the assumption that $\Delta P_{cap}$ is equal to $\Delta P_{liq}$, one can now take the expressions for these variables and substitute them into:

$$\dot{Q} = \dot{m} h_{fg}$$

Where $\dot{m}$ is the mass flow through the heat pipe and $h_{fg}$ is the latent heat of evaporation. This then gives an expression for $\dot{Q}$ that can be maximized, in order to maximize heat transfer.

Considering that the maximum heat flow of the heat pipe would be limited by a wick and given that the heat transfer through the heat pipe should be maximized, it is chosen to not use a wick. By doing so, the maximum heat flow is higher, but the derivation of the Figure of Merit is dependent on other factors. To derive a Figure of Merit, it useful to take a look at figure 2.15. This figure will be further explained in paragraph 2.6, but for now it suffices to recognise that the resistances $z_3$ and $z_7$ dominate the resistance scheme. This assumption will later be substantiated, but for now we assume this to be true. In order to maximize the heat transfer through the thermosyphon, one should minimize the thermal resistance across the liquid film by choosing the liquid wisely. The overall heat transfer coefficient across condensing vapour into a downflowing liquid film is given by Nusselt's theory of filmwise condensation [15] (formula 7.16 Mills):

$$\overline{h} = 0.943 \left[ \frac{h_{fg} g(\rho_l - \rho_v) k_l^3}{L(T_{sat} - T_w)\nu_l} \right]^{1/4} \tag{2.3}$$

Where $\overline{h}$ is the overall heat transfer coefficient, $g$ is the gravitational constant, $\rho_l$ and $\rho_g$ stand for the density of the liquid and gas phase respectively, $k_l$ is the thermal conductivity of the liquid, $L$ is the total height of the film, $T_{sat}$ is the saturation temperature of the fluid, $T_w$ is the wall temperature and $\nu_l$ is the kinematic viscosity of the liquid. To simplify the equation, we cross out the terms that do not depend on the working fluid: $L$, $T_{sat}$, $T_w$ and $g$. Furthermore, since $\rho_l \gg \rho_v$, we cross out $\rho_v$. We can also convert the kinematic viscosity into dynamic viscosity using: $\nu_l = \mu_l / \rho_l$, where $\mu_l$ is the dynamic viscosity. Applying all of the above to equation 2.3 gives [3][18]:

$$FoM = \left[ \frac{h_{fg} k_l^3 \rho_l^2}{\mu_l} \right]^{1/4} \tag{2.4}$$

Where $FoM$ is the Figure of Merit that should be maximized in order to maximize the total heat transfer capabilities of the heat pipe. However, there are some points of caution:

1. The Figure of Merit is only useful if the total heat transfer is solely limited by the resistance across the condensing film. This means that the hydrostatic pressure loss should be relatively small. Especially for geothermal applications, when the heat pipe is scaled up to hundreds of meters length, this assumption is not valid.

2. It is only valid if the total heat transfer is well below the theoretical heat transfer limits discussed in paragragph 2.5.

3. We assume that there is filmwise condensation within the heat pipe, but it could very well be that there is dropwise condensation (later on we will see that this is not the case).

4. The Figure of Merit does not concern itself with whether the working fluid is compatible with the material the heat pipe is made of and the vapour pressure of the working fluid.

Keeping these considerations in mind, we now take a look at common working fluids for heat pipes. ESDU released a paper [20] in which they simulated for different fluids the Figure of Merit for a wide range of temperatures. From figure 2.11, it can be seen that for a temperature range of 15-350 $^o$C, water is the substance with the highest Figure of Merit. By taking water as a working fluid, we ensure that the maximum amount of heat can be transported for the temperature range given at the beginning of this chapter.

### 2.4.1. Low pressure challenges

Choosing water as our working fluid, gives certain challenges. The main one is keeping the setup at low pressures (low pressure in the context of this paragraph means 20-30 mbar) such that the operating conditions in the heat pipe match the vapour pressure of water. Another question the author received was whether the heat pipe would be able to withstand low pressures. Would the glass section not implode or explode? To check if the tubes will implode under vacuum conditions, one can use the following formula [26]. This formula predicts what under what external pressure a thin-walled tube will collapse:

$$p = \frac{2E}{1-\tau^2}(t/D)^3 \tag{2.5}$$

Where $p$ is the external collapsing pressure, $E$ is the modulus of elasticity, $\tau$ is the Poisson's ratio, $t$ is the thickness of the wall and $D$ is the diameter of the tube. Taking property values from CES Edupack [4], for a 54 mm copper pipe with a 1.5 mm wall thickness, the outside pressure can be 64 bar, which is more than enough to withstand low pressure conditions. For common Pyrex glass tubes with a 2.5 mm thick wall, this number is around 130 bar. Which is much more than needed. This has to do with the fact that glass is excellent at withstanding compressive forces, while it has poorer performance for tensile forces. To check if the pipe will explode when a crack is formed through the pipe, we will use the 'leak-before-break' criterion. This number gives an estimation of what overpressure the pipe can handle when there is a crack that penetrates through the complete pipe wall [5]:

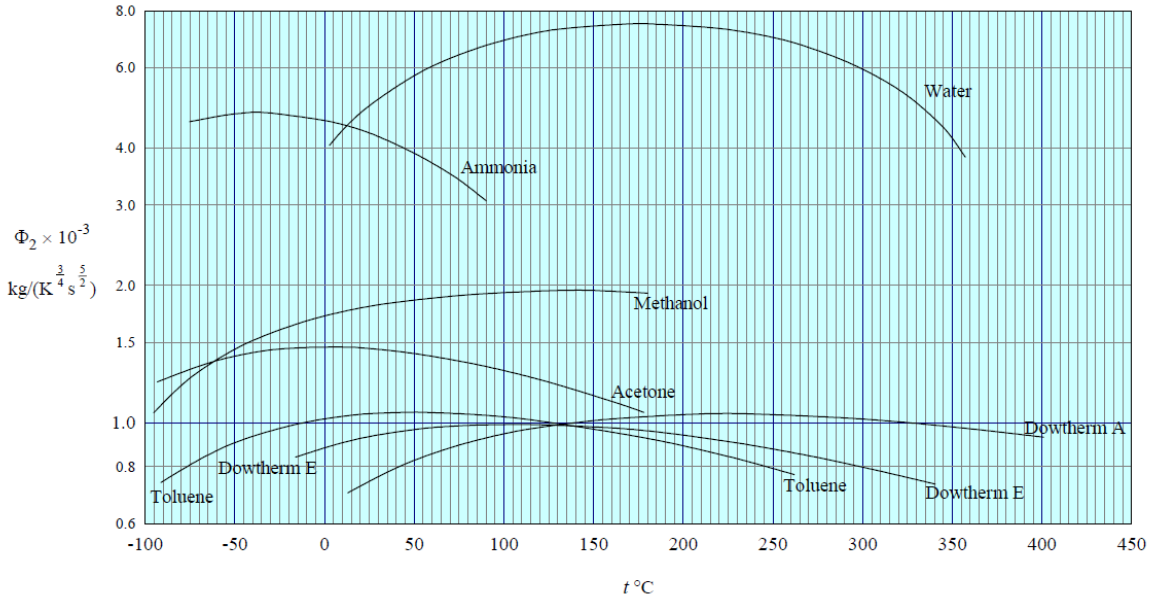


Figure 2.11: Figure of Merit for two-phase thermosyphons [20]

$$p \leq \frac{4Y}{\pi R} \frac{K_{1c^2}}{\sigma_y} \tag{2.6}$$

Where $Y$ is a constant and generally equal to 1, $R$ is the radius of the pipe, $K_{1c}$ is the fracture toughness and $\sigma_y$ is the yield strength. If we now take numbers from CES Edupack, the maximum overpressure it can handle is around 6 bar overpressure, which is more than enough for the setup. After all, the saturation temperature of water at 7 bar absolute pressure is 165 $^o$C [17]. However, to make sure this pressure is never reached a safety valve is added in the setup that will blow off steam at 3 bar absolute pressure. The maximum operating temperature is therefore 130 $^o$C. As a second safe measure, a blast resistant, plastic film is added around the glass pipe sections.

Now that the working fluid and the rough dimensions are established, we can check whether they are able to support the requirements that were postulated at the beginning of this chapter. To this end, two different methods are employed:

1. Comparing the dimensions of the heat pipe with various theoretical limits.
2. The thermal resistance method: calculating unknown temperatures by evaluating the temperature drop over the thermal resistances in the setup.

## 2.5. Theoretical heat transfer limits

In order to get an initial guess on whether the desired heat throughput is viable, we use two papers from ESDU [3][1]. In these papers, the various heat transfer limits are discussed. In figure 2.12, one can see the different limits that one might encounter. We will now discuss each limit one by one.

### 2.5.1. Viscous limit

The viscous (or vapour pressure) limit is encountered when the operating temperature and pressure are relatively low (~0.1 bar). The viscous limit means that the pressure in the top of the heat pipe approximates vacuum conditions because of the pressure losses within the heat pipe due to friction. If the heat fluxes through the heat pipe increase, the speed of the vapour through the heat pipe needs to increase. This gives higher friction losses at the wall of the heat pipe. The viscous limit tries to put a number on the limit of heat transfer for different operating pressures. For an analytical derivation please refer to Busse [6]. The viscous heat transfer limit is given as [1]:

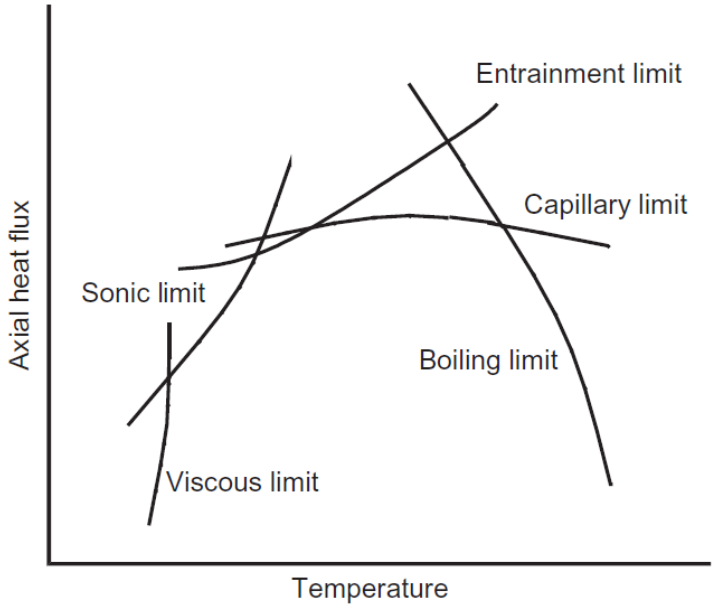


Figure 2.12: Plot of the theoretical heat transfer limit envelope [18]

$$\dot{Q}_{vis} = \frac{A_e D_i^2 h_{fg}}{64 \mu_v l_{eff}} \rho_v P_v \tag{2.7}$$

Where $A_e$ is the cross-sectional area of the evaporator, $D_i$ is the inside diameter of the heat pipe and $l_{eff}$ is the effective length of the heat pipe. The effective length is defined as:

$$l_{eff} = l_e/2 + l_a + l_c/2$$

With $l_e$ being the length of the evaporator section, $l_a$ the length of the adiabatic section and $l_c$ the length of the condenser.
We can now fill in equation 2.7 using numbers obtained from the NIST database using the computer program Refprop [17]. The operating temperature range is defined as 50-80 $^o$C. The viscous limit is the lowest for the lowest temperature. We therefore use 50 $^o$C to calculate this limit. Filling the numbers obtained from Refprop into equation 2.7 gives:

$$\dot{Q}_{vis} = \frac{(\pi(25.5 \bullet 10^{-3})^2)(51 \bullet 10^{-3})^2 2383}{64(10.511 \bullet 10^{-6})7.37}(8.2567 \bullet 10^{-2})(1.226 \bullet 10^4) = 2585 kW \tag{2.8}$$

This result means that the pressure losses in the heat pipe due to viscous friction losses are negligible. To check if this result makes any sense, we can employ another method to calculate the viscous pressure losses. Let us assume that 10 kW of heat comes in at the evaporator section, then the mass of water that is evaporated every second is:

$$\dot{m} = \frac{\dot{Q}}{h_{fg}}$$

Now we convert mass to volume by dividing the right-hand side by density. To further convert the volume flow to a speed, we divide the right-hand side by cross-sectional area. This then gives the average speed of the vapour that goes through the heat pipe:

$$v_v = \frac{\dot{Q}}{h_{fg} \rho_v A_e} \tag{2.9}$$

Where $v_v$ is the average vapour speed. Now filling in the numbers obtained from Refprop [17]:

$$v_v = \frac{10}{2383(8.2567 \bullet 10^{-2})(\pi(25.5 \bullet 10^{-3})^2)} = 24.9 m/s$$

The Reynolds number is defined as:

$$Re \equiv \frac{\rho_v v_v D_i}{\mu_v} \tag{2.10}$$

Filling in the data from Reprop into equation 2.10:

$$Re = \frac{(8.2567 \bullet 10^{-2})24.9(51 \bullet 10^{-3})}{10.511 \bullet 10^{-6}} \approx 10^4$$

Since $Re > 2100$, the flow must be turbulent [18]. The frictional pressure loss is then given by the Fanning equation:

$$\frac{P_1 - P_2}{l} = \left(\frac{4}{D_i}\right) f \left(\frac{1}{2}\right) \rho_v v_v^2 \tag{2.11}$$

Where $f$ is the Fanning friction factor. For turbulent flows it can be related to the Reynolds number as:

$$f = \frac{0.0791}{Re^{1/4}}$$

If we now substitute this expression into equation 2.11 and fill in the values given by Refprop:

$$\Delta P = \left(\frac{4l}{D_i}\right)\left(\frac{0.0791}{Re^{1/4}}\right)\left(\frac{1}{2}\right)\rho_v v_v^2 = \left(\frac{4 \bullet 9}{51 \bullet 10^{-3}}\right)\left(\frac{0.0791}{(10^4)^{1/4}}\right)\left(\frac{1}{2}\right)(8.2567 \bullet 10^{-2})24.9^2 = 143 Pa$$

This would be the pressure loss over the heat pipe if the fluid was flowing from the bottom to the top, while the hydrostatic pressure is neglected. Compared to the saturation pressure of water at 50 $^o$C (12260 Pa) this number is insignificant, which confirms the hypothesis that the viscous pressure limit will not be the critical heat transfer limit.

### 2.5.2. Sonic limit

During operation the vapour flowing through the heat pipe might reach such a velocity that it approaches the sonic speed. This is something to be especially cautious about during the start-up phase. When the temperatures are relatively low, the density of the vapour phase is low as well. For example, below 45 $^o$C the density of saturated water vapour is in the order of 0.01 kg/m$^3$, which is detrimental to the heat flow. It can be seen from equation 2.9 that the lower the density, the higher the speed of the vapour phase through the heat pipe will be. To check if the sonic limit will be encountered, two different formulae are used. The first one comes from Busse [6]. For an analytical derivation, please refer to that paper. The limit is given as:

$$\dot{Q}_{son} = 0.474 A_e h_{fg} (\rho_v P_v)^{1/2} \tag{2.12}$$

Again, we can now take the numbers obtained from Refprop for water at 50 $^o$C and feed them into equation 2.12. This then yields:

$$\dot{Q}_{son} = 0.474 \left[\pi(25.5 \bullet 10^{-3})^2\right] 2383 \left[(8.2567 \bullet 10^{-2})(1.226 \bullet 10^4)\right]^{1/2} = 73.4 kW$$

This results suggests that the flow will not reach choked conditions. To be sure, another way of calculating an ESDU paper can be used [1]:

$$\dot{Q}_{son} = \frac{A_e a h_{fg} \rho_v}{\sqrt{2(1+\gamma)}} \tag{2.13}$$

Where $a$ is the speed of sound through the vapour and $\gamma$ is the specific heat ratio. If we now fill in the numbers obtained from Refprop:

$$\dot{Q}_{son} = \frac{\left[\pi(25.5 \bullet 10^{-3})^2\right] 443.11 \bullet 2383(8.2567 \bullet 10^{-2})}{\sqrt{2(1+1.3277)}} = 82.5 kW$$

This is the same order magnitude as the result that was obtained earlier. To be really sure, we can compare the vapour speed in the heat pipe with the theoretical speed of sound. At 50 $^o$C, the vapour speed is 24.9 m/s

(equation 2.9), while the speed of sound under those conditions is 433.11 m/s. The Mach number then is 24.9/433.11 = 0.06, which is indeed well below choking conditions.

### 2.5.3. Entrainment limit

In the heat pipe there is a counter-current flow of vapour going to the condenser, while liquid comes down to the evaporator. Entrainment of liquid can occur if the vapour velocity is so high that it peels liquid off the wall. The relatively high velocity at the vapour-liquid interface gives a shear stress at the interface. This stress can induce large surface waves at the interface, which leads to instabilities in the flow. The instabilities lead to entrainment of the liquid in the vapour flow. Instead of going to the evaporator, the liquid is now transported to the condenser. In a severe case, this can lead to dry-out of the evaporator. Even if dry-out does not occur, it still limits the flow of liquid from the condenser to the evaporator.
The entrainment limit is not exactly defined and not trivial to predict. Therefore the conditions at which the heat transfer limit is defined is the moment at which entrainment begins. For this end we employ two different equations. The first equation comes from Sakhuja and seems to match the experimental results from Groll [16]:

$$\dot{Q}_{ent} = C_w^2 \left( \frac{D_i^{2.5}\pi}{4} \right) \frac{h_{fg}\sqrt{g\rho_v(\rho_l - \rho_v)}}{\left[1 + (\rho_v/\rho_l)^{0.25}\right]^2} \tag{2.14}$$

Now filling in the numbers for water at 50 $^o$C and $C_w$=0.725:

$$\dot{Q}_{ent} = 0.725^2 \left( \frac{(51 \bullet 10^{-3})^{2.5}\pi}{4} \right) \frac{2383\sqrt{9.81(8.2567 \bullet 10^{-2})(988.06 - 8.2567 \bullet 10^{-2})}}{\left[1 + (8.2567 \bullet 10^{-2}/988.06)^{0.25}\right]^2} = 13.6kW$$

This is an alarming value, since the desired heat throughput is 10 kW. However, Sakhuja takes $C_w$ to be 0.725 for vertical heat pipes, but Groll advises $C_w$ to be 1.105, which would result in $Q_{ent}$=31.6 kW.

The second method of calculating the entrainment limit is from an ESDU paper [3]. The formula is similar to equation 2.14, but it is slightly more advanced:

$$\dot{Q}_{ent} = A_e h_{fg} f_1 f_2 f_3 (\rho_v)^{0.5} [g(\rho_l - \rho_v)\sigma]^{0.25} \tag{2.15}$$

Where $\sigma$ is the surface tension and $f_1$, $f_2$ and $f_3$ are parameters that can be read from figures in the ESDU paper. It is beyond the scope of this paper to dive any further into the theory behind these numbers. It is sufficient to know that $f_1$ = 8.2 and $f_3$ = 1 for vertical heat pipes. $f_2$ is given as:

$$f_2 = \left[ \frac{p_v}{[g(\rho_l - \rho_v)\sigma]^{0.5}} \right]^{-0.17}$$

Filling in these numbers into equation 2.15 gives $Q_{ent}$ = 20.3 kW. This number is in between the results from Groll and Sakhuja.

As said at the beginning of this paragraph, the entrainment limit is hard to define and predict. The true value of where entrainment begins will probably be somewhere in the middle. However, based on the numbers that are obtained up until now, it seems like the heat pipe can attain its desired performance.

### 2.5.4. Boiling limit

The boiling (or burnout) limit is encountered when the temperature of the evaporator wall is relatively high compared to the liquid temperature in the evaporator. This boiling limit occurs only for if there is a pool present in the evaporator. At the wall, vapour bubbles are formed. The higher the heat flux, the more bubbles are formed. It has been observed that at a critical heat flux the bubbles come together and form a vapour film which limits the flow of liquid towards the wall. This film then insulates the wall from the liquid and thus limits the heat flow [16]. In figure 2.13 it can be seen that with an increasing temperature difference between the evaporator wall and the liquid in the evaporator, the heat flux increases as well up until a certain point. This is the critical heat flux. Beyond this point lies the transition regime. This is the unstable part of the curve. The temperature difference increases but the wall cannot release its heat to the fluid. Which makes the temperature of the wall rise even more. This is a positive feedback loop, which can lead to extreme wall temperatures and ultimately damage of the equipment.

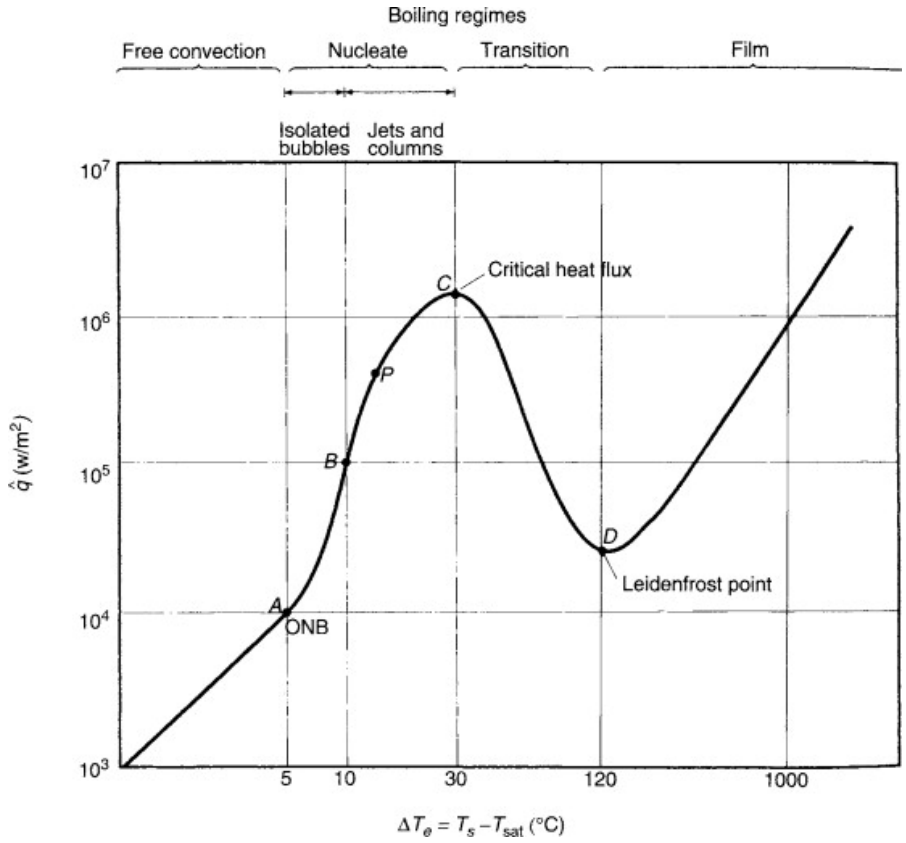


Figure 2.13: Characteristic boiling curve for water [12]

EDSU gives the boiling limit as [3]:

$$\dot{Q}_{bo} = 0.12 h_{fg} S_e (\rho_v)^{0.5} [\sigma g(\rho_l - \rho_v)]^{0.25} \tag{2.16}$$

Where $S_e$ is the internal surface area of the evaporator. For water at 50 $^o$C, formula 2.16 gives 40 kW, which is well below 10 kW.

### 2.5.5. Dryout limit

Dryout can occur if the amount of liquid in the evaporator becomes too low. The heat that is provided then can not be absorbed by the liquid. Hence, the amount of the heat that can be transferred through the heat pipe is limited. EDSU [3] gives as a rule of thumb that the filling ratio (FR) should be at least 50%. FR is defined as:

$$FR = \frac{V_l}{V_e}$$

Which stands for the ratio of the liquid in the evaporator ($V_l$) versus the total volume of the evaporator ($V_e$). If the FR should be higher than 50%, then for a 51mm I.D. pipe and a height of 0.5 meters, the minimum volume of liquid in the evaporator should be 0.5 liter. The ESDU paper gives second directive for what the liquid volume should be:

$$V_l = 0.001 D_i l$$

Where $l$ is the total length of the evaporator. The formula gives an indication what the liquid volume should be if the wall of the heat pipe is covered in a 0.3 millimeter thick liquid film. The 0.3 millimeter is a rough estimate for typical film thicknesses. One can check if this number is correct using formula 7.14 from Mills [15]. Given that the total length of the heat pipe is around 9 meters and the inner diameter of the pipe is 51 millimeter, the formula given above then gives 0.46 liter. Both aforementioned formulae suggest a FR of about 0.5 liters, which will be followed.

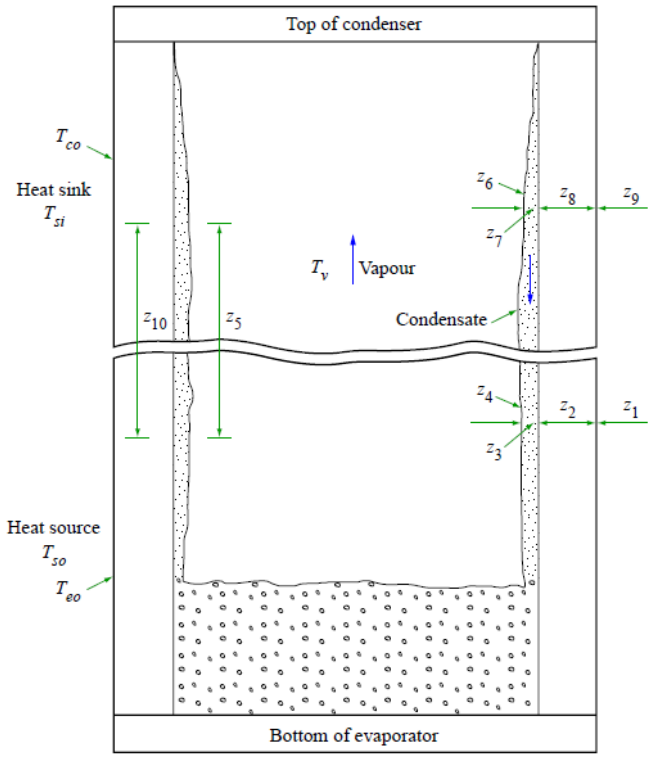


Figure 2.14: Location of thermal resistances [2]

### 2.5.6. Capillary limit

The more observant amongst the readers may have noticed that the capillary limit is not discussed, while it is mentioned in figure 2.12. The capillary limit is only relevant for wicked heat pipes. It gives the maximum heat flux if it is limited by the amount of liquid that can flow through the wick. Since the thermosyphon is wickless, it is not further discussed.

## 2.6. Thermal resistance method

The idea behind this method is to check whether the heat pipe does not contain thermal resistances that are too great to overcome. A thermal resistance indicates what temperature drop will result from heat transfer through a certain medium or to another medium. A schematic overview of where the thermal resistances are located can be found in figure 2.14. From this picture a more abstract, schematic overview can be made which can be seen in figure 2.15.

### 2.6.1. Evaporator resistances

The first heat resistance that is encountered is the resistance ($z_1$) to get from the heat source to the outside of the evaporator wall. This resistance is dependent on how one is going to heat the evaporator section. For the heat pipe discussed in this paper, a band heater was used. Typical interfacial conductance coefficients for metal on metal contact are in the order of 1,000 to 10,000 $W/(m^2K)$ [15]. However, Mills also states: 'The contact resistance can be the dominant thermal resistance when high-conductivity metals are involved.' Later on we will see how painfully true this statement is. For now, we assume that the interfacial conductance coefficient is ~1,000 $W/(m^2K)$. One more consideration is the fact that the band heaters do not heat the area around the terminals and mounting holes. Therefore, a smaller contact area is taken.

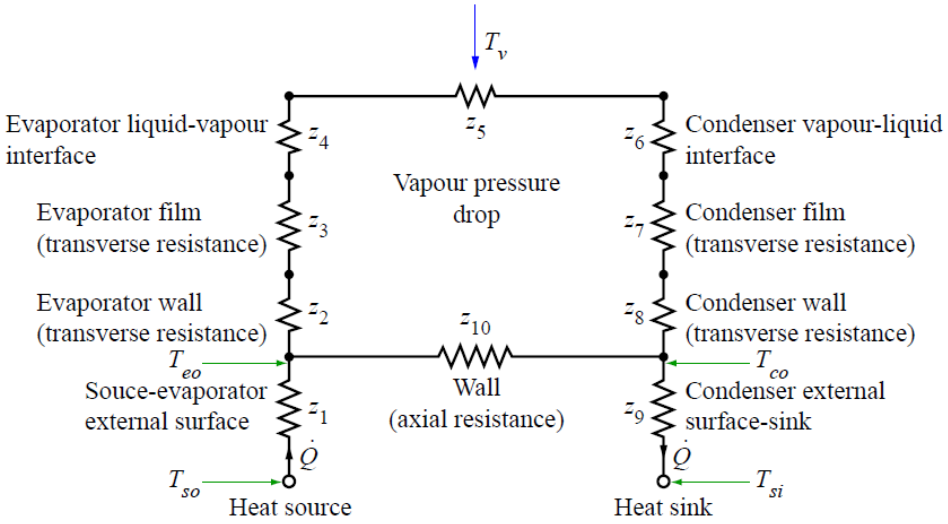


Figure 2.15: Schematic of the thermal resistances [2]

From figure 2.15 one can see that there are two different resistances connected to $z_1$. First we look at $z_{10}$: the wall resistance. This resistance is given by a modified form of Fourier's law of conduction:

$$z_{10} = \frac{l}{kA} \tag{2.17}$$

With $A$ being the cross-sectional of the copper tube. The area can be calculated by:

$$A = \pi * (R_o^2 - R_i^2)$$

With $R_o$ being the outside radius and $R_i$ being the inside radius of the heat pipe. In this case $R_o$ = 27 mm and $R_i$ = 25.5 mm. This then gives A = 247.4 mm$^2$. The heat pipe is around 10 meters high. We now assume that the complete pipe is made from copper, with a thermal conductivity coefficient of 400 W/(mK). Feeding these values into equation 2.17, gives:

$$z_{10} = \frac{10}{400 * (247.4 * 10^{-6})} = 101 K/W \tag{2.18}$$

Which is multiple orders of magnitude greater than the sum of all other resistances combined. For further simplification this resistance is set to be infinite.

Resistance 2 ($z_2$) is the resistance across the wall of the evaporator. This resistance is given by Mills as:

$$z_2 = \frac{\ln(R_o/R_i)}{2\pi k l_e} \tag{2.19}$$

Sine the material used is copper, and the thickness of the wall 1.5 mm, the resistance across the wall is so small (order $10^{-5}$ K/W) it is not further considered.

Now we arrive at a more interesting part of the heat journey: the resistance across a liquid film or the pool boiling resistance. The inside of the wall of the evaporator is either exposed to a pool or a falling film of fluid depending on the filling ratio.

### 2.6.2. Pool boiling resistance

For pool boiling, Mills gives the Rohsenow correlation as a measure for the heat transfer coefficient. Mills does give a warning: 'Equation (...) is not very accurate, however, and errors of 100% (!) in $q$ and 25% in $\Delta T$.'

[15] Since we are not interested in values with an error of 100% we do not consider the Rohsenow equation any further. ESDU mentions the work of Shiraishi [3][19]. Shiraishi gives the pool boiling resistance as:

$$z_{3,p} = \frac{1}{\Phi g^{0.2} \dot{Q}^{0.4} (\pi D_i l_e)^{0.6}} \tag{2.20}$$

Where $\Phi$ is defined as:

$$\Phi = 0.32 \frac{\rho_l^{0.65} k_l^{0.3} c_{pl}^{0.7}}{\rho_v^{0.25} h_{fg}^{0.4} \mu_l^{0.1}} \left[ \frac{p_v}{p_a} \right]^{0.23}$$

The physical fluid properties of this expression are evaluated at atmospheric boiling conditions. The last term in $\Phi$ ($\left[p_v/p_a\right]^{0.23}$) is there to correct for the pressure in the heat pipe. For water, $\Phi$ then becomes:

$$\Phi = 63(p_v/p_a)^{0.23}$$

Feeding this expression into equation 2.20 then gives:

$$z_{3,p} = \frac{1}{63(p_v/p_a)^{0.23} g^{0.2} \dot{Q}^{0.4} (\pi D_i l_e)^{0.6}} \tag{2.21}$$

The pool boiling resistance at vapour pressures of around 50-100 mbar, is about $2 \bullet 10^{-3}$ K/W.

One remark about equation 2.20 is that it is only valid for smooth pipes. By roughening the inside of the pipe, one can increase the heat transfer by a factor of 2 to 3.

### 2.6.3. Liquid film resistance

To get an idea of what the liquid film will look like (e.g. is it wavy, smooth or has it dry patches) it is useful to look at the Reynolds number of the film. The Reynolds number is given by ESDU as [3]:

$$Re_f = \frac{4\dot{Q}}{h_{fg} \mu_l \pi D_i}$$

(Please note that ESDU made a 'mistake' by printing $\mu_l$ as $\mu l$. One can do dimensional analysis or derive the Reynolds number for themselves to verify.) For vapour temperatures of 30-50 $^o$C, the Reynolds number is in the range of 130-200. This range is typical for wavy laminar flow [3][15]. ESDU now states: 'thermal resistance is reduced by the formation of waves on the surface of a film.' Hence, the thermal resistance that is about to be calculated might be a good portion bigger than the actual thermal resistance. We now use two different methods to get the resistance over the liquid film. The first method is to take the Nusselt's theory of filmwise condensation and apply it to filmwise evaporation. This theory assumes an absolute worst-case scenario because it does not take the waves on the free surface into account. ESDU gives a rewritten version of the filmwise condensation equation and since ESDU does recommend this formula we will take a closer look at it. The second method is using a slightly more advanced formula from Mills that does take the wavy nature of the free surface into account.

For the first method we take a look again at formula 2.3:

$$\overline{h} = 0.943 \left[ \frac{h_{fg} g (\rho_l - \rho_v) k_l^3}{L (T_{sat} - T_w) \nu_l} \right]^{1/4}$$

Given that the vapour temperature is in the range of 30-50 $^o$C, the averaged heat transfer coefficient is around $5 \bullet 10^3$ W/m$^2$K. Converting this heat transfer coefficient to thermal resistance using:

$$z_{3,f} = \frac{1}{\overline{h} A_{i,e}}$$

Where $A_{i,e}$ is the internal wall area of the evaporator. Giving in $5 \bullet 10^3$ W/m$^2$K then results in a thermal resistance of $2.5 \bullet 10^{-3}$ K/W.

Similarly, ESDU rewrites formula 2.3 in a format where one directly obtains the resistance across the film [3]:

$$z_{3,f} = \frac{0.235\dot{Q}^{1/3}}{D_i^{4/3} g^{1/3} l_e FoM^{4/3}} \tag{2.22}$$

Where $FoM$ is the Figure of Merit, as described in equation 2.4.

The second method one can employ is to take the formula for wavy laminar film condensation and apply it to wavy laminar film evaporation (see figure 2.16 for a picture of a wavy laminar flow). Mills gives the following equation (equation 7.30 in Mills):

$$\overline{Nu} = \left[ \frac{Pr_l}{4Ja_l} \frac{(\nu_l^2/g)^{1/3}}{L} \right]^{0.18} \tag{2.23}$$

Where $\overline{Nu}$ is the averaged Nusselt number, $Pr_l$ is the Prandtl number of the liquid and and $Ja_l$ stands for the Jakob number. The Jakob number is defined as:

$$Ja_l = \frac{c_{pl}(T_{sat} - T_w)}{h_{fg}}$$

Feeding in similar numbers as in equation 2.3, the averaged Nusselt number is about 0.34. Converting this number into a thermal resistance:

$$z_{3,f} = \frac{(\nu_l^2/g)^{1/3}}{k_l \overline{Nu} A_{i,e}} \tag{2.24}$$

Which gives $z_{3,f}$ to be around $2 \bullet 10^{-3}$ K/W. Compared to the result obtained before ($2.5 \bullet 10^{-3}$ K/W), the wavy laminar film resistance is 20% smaller. This result is in accordance with what is stated in literature and hence gives us more confidence in the validity of the results.

### 2.6.4. Condenser resistances

In the condenser similar processes play a role as in the evaporator. The resistance across the film can be calculated using formulae 2.23 and 2.24. The only difference is that the wall is now colder than the fluid. Also, since the condenser should not be the limiting factor in the setup, the author saw it fit to oversize the condenser. This makes it possible that the condenser dictates what the conditions are in the heat pipe. For low flows of cooling water, the vapour temperature in the heat pipe will go up. While for higher flows, the vapour temperature goes down. The resistance across the liquid film in the condenser is about $5.7 \bullet 10^{-4}$ K/W.

The resistance across the wall of the condenser can be calculated using formula 2.19. Given that the length of the condenser is 2.5 meters instead of the 0.5 meters of the evaporator, the wall resistance is about $9 \bullet 10^{-6}$ K/W.

The resistance at the interface of the wall and the cooling water is highly dependent on the mass flow of the coolant. For higher mass flows, a more turbulent flow will develop along the wall of the condenser and will in turn give a higher heat transfer coefficient. Also, the temperature of the coolant will be lower along the pipe for higher mass flows, which will facilitate a better heat flow. However, to still put some number on this convective resistance, we will assume a heat transfer coefficient of 2,000 W/m$^2$K. The author checked this number using formula 4.65 from Mills. The heat transfer coefficient can then be converted to a thermal resistance using:

$$z = \frac{1}{h \bullet A_i} \tag{2.25}$$

Which results in a $z_9 = 1.24 \bullet 10^{-3}$ K/W

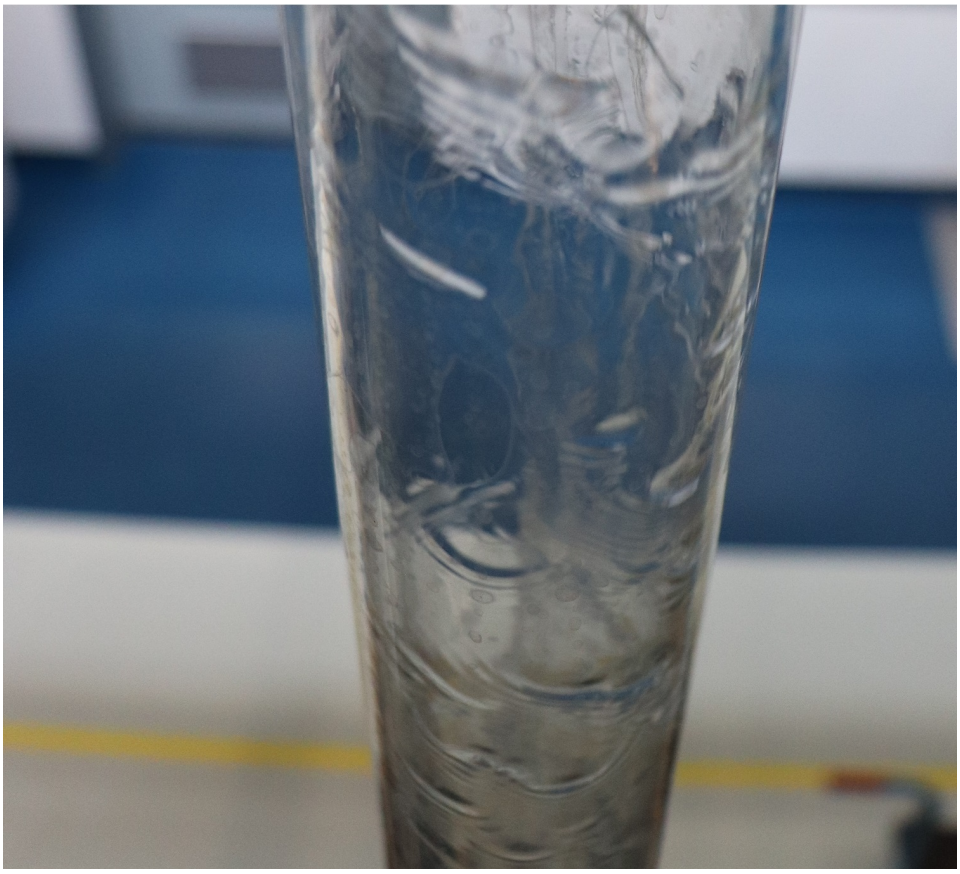

Figure 2.16: Picture of the wavy laminar flow in the heat pipe.

### 2.6.5. Conclusions

It is now useful to put all the numbers obtained in an overview as shown in table 2.2

A few remarks considering not all numbers that are mentioned in figure 2.15 are given in the table above. The resistances $z_4$ and $z_6$ stand for the resistance from the liquid-vapour interface in the evaporator and condenser respectively. Those resistances are usually extremely small (order $10^{-5}$) and have no real impact on the performance of the heat pipe [3]. The vapour pressure drop that is represented by $z_5$ is also extremely small as we already have seen from equation 2.11.

Now that this is settled, we can see that the resistance across the copper tubing are negligible. What seems to be problematic is that the $z_1$ is bigger than all of the other resistance combined. The total resistance is around $1.6 \bullet 10^{-2}$ K/W. This means that $z_1$ makes up for 76% of the total resistance. Also, if the total resistance really would be this high, the total temperature drop over the heat pipe would be around 160 $^o$C, while the idea is to simulate geothermal heat, which goes up to 80 $^o$C. Ideally, the total resistance of the heat pipe is

| **Resistance** | **Value [K/W]** | **Formula** |
|---|---|---|
| $z_1$ | $1.24 \bullet 10^{-2}$ | - |
| $z_2$ | $10^{-5}$ | 2.19 |
| $z_{3,p}$ | $2 \bullet 10^{-3}$ | 2.21 |
| $z_{3,f}$ | $2 \bullet 10^{-3}$ | 2.24 |
| $z_7$ | $5.7 \bullet 10^{-4}$ | 2.24 |
| $z_8$ | $9 \bullet 10^{-6}$ | 2.19 |
| $z_9$ | $1.24 \bullet 10^{-3}$ | 2.25 |
| $z_{10}$ | $10^2$ | 2.17 |

Table 2.2: Overview of the calculated resistances

lower than $(80-20)/10000 = 6 \bullet 10^{-3}$ K/W. What the consequences are of these numbers, we will see in the next chapter.

# 3

# Results

## 3.1. Calibration

Three different measurement devices have to be calibrated. The PT-100 thermometers have been calibrated at the factory, but to be sure their temperature readings are verified. First, the PT-100 is put in icy water. Next to the PT-100 a calibration thermometer is put, to check if the icy water is indeed 0 $^{o}$C. The calibration thermometer gave in all 4 tests a temperature of 0.013 $^{o}$C. Next to the thermometer the PT-100s are placed which all gave a temperature of 0.0 $^{o}$C, or in the case of TT-11 (see figure 2.1 for location) it gave 0.1 $^{o}$C. To check if the PT-100s will be reliable at operation temperature, the PT-100s are placed in a stove. The results are shown below:

| **Sensor number** | **Calibration temperature [$^{o}$C]** | **PT-100 measurement[$^{o}$C]** |
|---|---|---|
| $TT-09$ | 59.50 | 58.9 |
| $TT-10$ | 59.42 | 58.7 |
| $TT-11$ | 100.22 | 100.1 |
| $TT-12$ | 100.15 | 100.0 |

Table 3.1: Temperature of the calibration thermometer versus the temperature given by the PT-100.

It is important to notice that the temperature given by TT-09 and TT-10 are slightly lower than the value from the calibration thermometer. This is due to the fact that TT-09 and TT-10 are both contact PT-100s, while TT-11 and TT-12 are PT-100s with a metal sheath. The contact PT-100s were put in the stove, but made no direct contact with the hot wall while the calibration thermometer did. Since no other method of verifying the measured temperatures was available, the values obtained were deemed to be satisfactory.

### 3.1.1. Pressure sensor

To calibrate the pressure sensor, a calibrated, more accurate pressure sensor was used (type Chell Barocell 622). The calibration sensor is inserted into the tube that leads to the vacuum pump. Now the vacuum pump is turned on and off at regular intervals, to compare the pressure of the calibration sensor and the pressure sensor in the setup. The results are as follows:

| **Calibration pressure [mbar]** | **Measured pressure [mbar]** |
|---|---|
| 802.0 | 801.8 |
| 494.0 | 492.3 |
| 226.6 | 224.3 |
| 100.0 | 96.7 |
| 52.5 | 50.3 |

Table 3.2: Pressure measured by the calibration sensor versus the pressure measured by the pressure sensor in the setup.

Using these numbers, one can plot the measurement error as shown in figure 3.1.

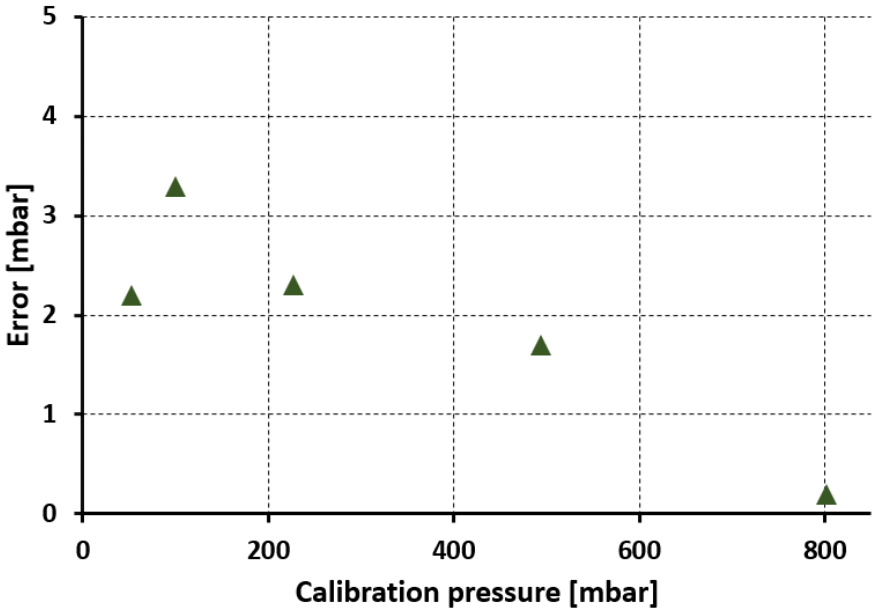


Figure 3.1: Calibration pressure versus the measurement error.

The pressure that is measured by the sensor in the setup is consistently underestimating the true value. However, since the accuracy of the setup sensor is only 0.6 mbar and the maximum error is 3.3 mbar, the results are deemed satisfactory.

### 3.1.2. Flow meter

To calibrate the flow meter, a large bucket was placed on scale. The flow of coolant was set to a certain value and after it reached a constant flow the outlet of the flow meter was pointed into the bucket. A stopwatch was started to measure the time that the outlet of the flow meter was pointed into the bucket. The results are as follows:

| Set flow [l/h] | Measured flow [l/h] | Average | Average error [l/h] |
|---|---|---|---|
| 250 | 233.9<br>228.2<br>227.3<br>232.9<br>238.6 | 232.2 | 17.8 |
| 500 | 467.2<br>466.5<br>465.6<br>463.4<br>477.6 | 468.1 | 31.9 |
| 1000 | 973.5<br>946.8<br>962.2<br>950.5 | 958.2 | 41.8 |
| 1750 | 1700.3<br>1711.5 | 1705.9 | 44.1 |

Table 3.3: The set flow on the flow meter versus the measured flow.

From this result is becomes clear that the flow sensor gives a value that is systematically too high. Especially at low flows, an error of 7% is unacceptable. To correct for the higher displayed flows a correction curve was made.

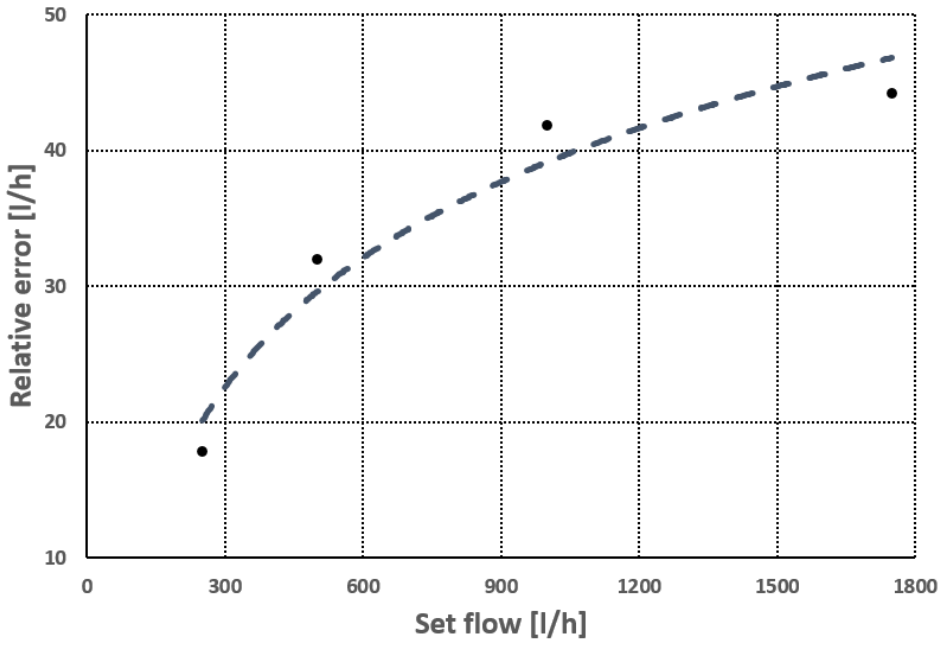


Figure 3.2: The set flow versus the averaged error. A logarithmic trend is visible.

In figure 3.2 one can see a logarithmic trend. The formula for the trend line is:

$$ER = 13.744 \bullet ln(SF) - 55.805$$

Where $ER$ is the average error and $SF$ is the set flow. To correct for the error that is introduced by the flow meter, one can simply subtract the expression mentioned above from the set flow.

## 3.2. Initial results

In the last chapter we left off with the conclusion that the interfacial heat transfer coefficient between the band heaters and the heat pipe might be too large to overcome. The initial results from the heat pipe can be seen in figure 3.3. Up until 100 seconds, one can see that the band heaters are gradually heating up. Between the 100 seconds and 200 seconds mark, one can see the overshoot that is caused by the PID controller. The power is somewhat lowered by the controller, to cool down the setup. Around the 220 second mark, a sharp dip is visible in the vapour temperature. This is due to an increase in the coolant flow. The PID controller responds by increasing the power output. When steady state is reached, one can see that the vapour temperature in the heat pipe is around 35 $^{o}$C, while the temperature of the band heaters is about 80 $^{o}$C. Also, the amount of power that the band heaters can get through the heat pipe, is significantly lower than expected. The heat pipe was designed to get an input temperature of 80 $^{o}$C and transport 10 kW of heat trough the pipe. However, there are two reasons that the heat pipe does not do its task:

1. The placement of the thermocouple in the band heater
2. The thermal resistance in between the band heater and the heat pipe.

### 3.2.1. Thermocouple placement

On the website of Watlow [25], the company states that the operating temperature goes up to 760 $^{o}$C. This is the first clue that the thermocouple might not be accurate and that the thermocouple is typically used at much higher temperatures. Also, the sheath of the band heater is made from stainless steel, which has a relatively low thermal conductivity (when compared to copper). From the pictures in the catalog it can be seen that the thermocouple is spot welded to the outside of the sheath. This means that the part of the sheath on the inside (the part that is in contact with the copper wall) might be much colder than the the outside of the

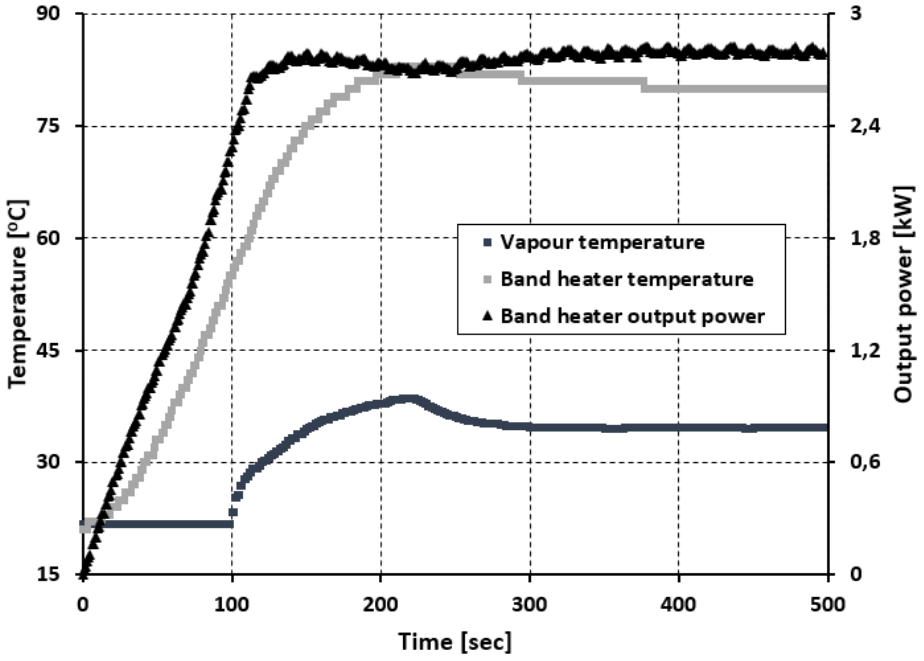


Figure 3.3: The initial performance of the heat pipe. Blue and green are temperatures, red is the heat output from the band heaters.

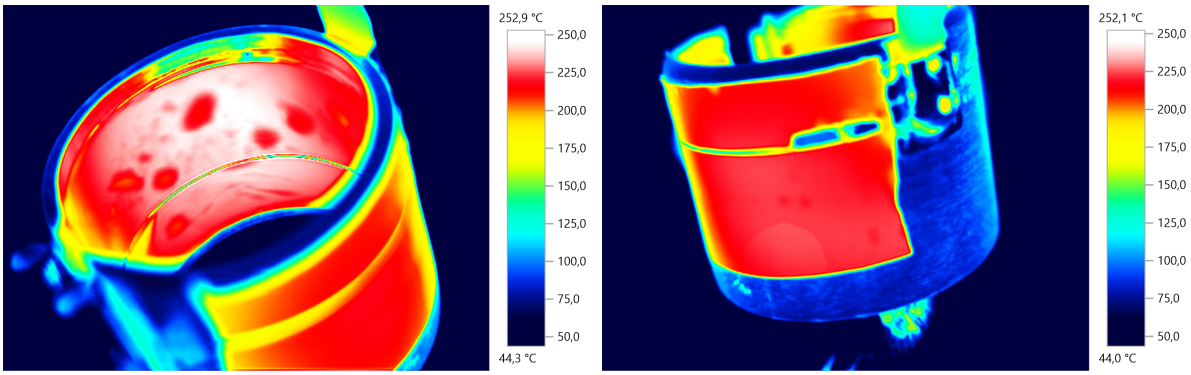


(a) The inside of a band heater

(b) Outside of a band heater

Figure 3.4: Two IR images of a band heater. Note that both color scales are the same, the pictures are taken directly one after the other.

sheath. To check if that is indeed the case, one of the band heaters is removed from the evaporator wall and studied with a thermal camera. Both the inside and the outside of the band heater are covered with infrared tape that has an emissivity of 0.95. The dark spots that one can see on figure 3.4a are from blisters under the tape because of the high temperature. The band heater is set at 220 $^{o}$C. One can see that the outside of the band heater is 220 $^{o}$C, while the inside is around 245 $^{o}$C. The main takeaway from this picture is that even though the band heater is exposed to air (which is a bad conductor) there is still a difference of 25 $^{o}$C between the outside of the band heater versus the inside. This indicates a thermal resistance between the inside and the outside of the band heater.

### 3.2.2. Interfacial thermal resistance

To further investigate the problem, measurements are done on the band heaters while they are in operation. The temperature of the band heaters is set to 80 $^{o}$C. The vapour temperature is 34 $^{o}$C. The temperature is measured with a calibrated thermocouple. The wall temperature is measured just above the band heater, while the band heater temperature is measured just besides the thermocouple pocket.

There are two peculiarities about these results: the first one is that the temperature that the thermocouple

| Element # | Wall temperature [$^o$C] | Band heater temperature [$^o$C] |
|---|---|---|
| 1 | 51 | 104.9 |
| 2 | 51 | 102 |
| 3 | 53.6 | 100 |
| 4 | 53 | 106.5 |
| 5 | 56 | 91 |
| 6 | 53 | 99.8 |
| 7 | 53 | 92 |
| 8 | 54 | 100 |

Table 3.4: Wall temperatures just above the band heaters and the temperature of the band heater outside sheath.

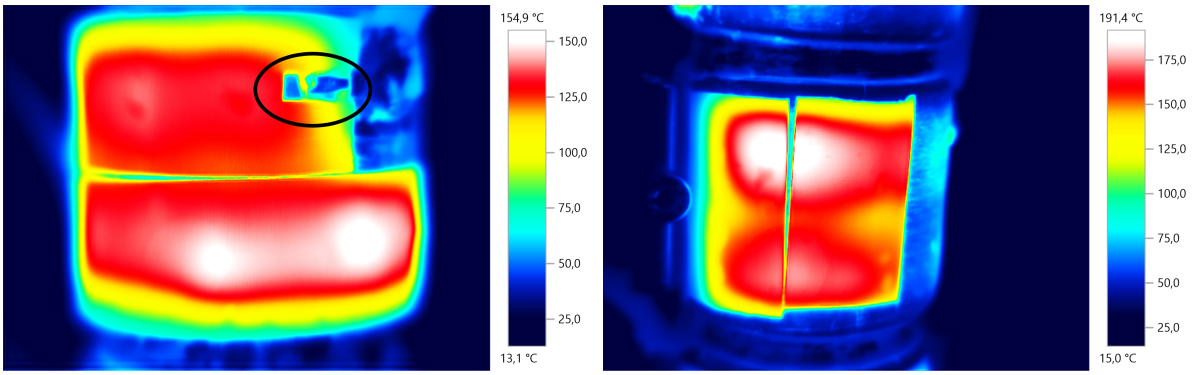


(a) TP around the thermocouple (circled region)

(b) TP on the outside of a band heater

Figure 3.5: Two IR images of a band heater whilst in operation. On both images a distinct Temperature Profile (TP) is visible

measures does not match with the value that the band heater measures. This, again, has to do with the thermocouple placement. It seems that around the thermocouple there is a cooler region. In figure 3.5a one can see a temperature gradient from left to right just above the thermocouple. This shows that the thermocouple of the band heater is placed on a colder region of the band heater sheath.

The second oddity is that there is such a temperature difference between the outside of the band heater and evaporator wall. This temperature difference is an indication that there is a significant thermal resistance between the evaporator wall and the outside of the band heater. In chapter 2.6.5 we already saw that the interfacial resistance between the evaporator wall and the band heater might be limiting the heat flow. To check if this is indeed the case, we first designate two potential causes: either the interfacial resistance of the evaporator wall and the band heater is limiting the heat flow, or the resistance across the wall to the vapour is. That last resistance can be easily checked since the data is given in table 3.4. The wall temperature is typically around 50 $^o$C and the vapour temperature is given as 34 $^o$C. From figure 3.3 it can be seen that the heat flow through the evaporator wall is about 2.8 kW. The resistance across the evaporator wall and the liquid film is then:

$$r = \frac{\Delta T}{\dot{Q}}$$

Which is about 5.7•10$^{-3}$ K/W. From table 2.2 it can be seen that $z_2$ and $z_{3,f}$ are in the same order of magnitude, but summed up they are a factor 2 smaller. Still, this can not account for the low heat transfer. The only logical conclusion from these results is that the resistance across the interface between the evaporator wall and the band heater is limiting the flow.

To check if this conclusion is indeed correct, a small test is made: one band heater is first covered in thermal paste (Omegatherm 201) and then placed back in the setup. A test run is done before the paste is applied and a test run afterwards. The results of this test can be found in figure 3.6. From this figure it is clear that the output power after the paste is applied, has increased significantly. Now that the cause has been identified, we put thermal paste on all the band heaters.

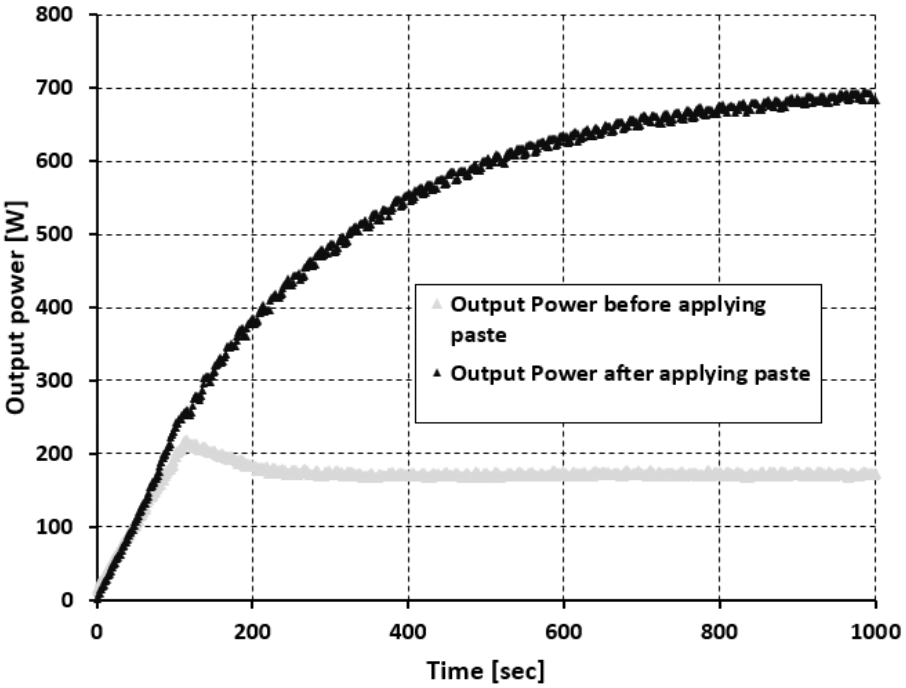


Figure 3.6: Performance of one band heater with and without thermal paste applied to its inside. Both times the set temperature of the band heater is 80 $^{o}$C.

Figure 3.7 shows us the performance after the thermal paste is applied to all band heaters. At a band heater temperature 80 $^{o}$C, the heat pipe still is not performing optimally. But where the heat pipe without thermal paste was could only get 2.8 kW through the pipe, now it can get 6 kW through. Keep in mind that the band heater temperature is measured on the outside of the band heaters and is not the true temperature of the band heaters.

## 3.3. Thermal losses

Now that the heat pipe can get to 10 kW of output power, the question is what the losses are in the pipe. The only power we have looked at up until now is the amount of electrical power that goes into the band heaters. A large part of the pipe has not been insulated. Not even the band heaters are insulated. In order to estimate how much heat is lost, the following experiment is set up: the band heaters are set at a temperature of 120 $^{o}$C, while the coolant flow is varied from 250 l/h to 1750 l/h. The idea is that for lower coolant flows, the vapour temperature in the heat pipe will rise. Higher vapour temperatures will make the uninsulated walls of the heat pipe hotter, which in turn will increase the thermal losses. Also, it is expected that since the band heaters are by far the hottest components, they will be a significant contributor to the thermal losses. So that even for low vapour temperatures (around 30-40 $^{o}$C) a good portion of the electrical power is lost to the environment. In figure 3.8a one can see the amount of power provided to the band heaters and the amount of heat that is extracted by the condenser. The amount of heat that is extracted is calculated using:

$$\dot{Q} = \dot{m} c_p \Delta T$$

Where $\Delta T$ is the temperature difference of the incoming and outgoing coolant and $\dot{m}$ is calculated by using:

$$\dot{m}\left[\frac{kg}{s}\right] = \frac{\dot{V}\left[\frac{l}{h}\right]\rho\left[\frac{kg}{m^3}\right]}{\left[\frac{3600s}{h}\right]\left[\frac{1000l}{m^3}\right]}$$

Where $\dot{V}$ is the volumetric flow rate. From figure 3.8a it becomes clear that the band heater output power and the power extracted by the condenser are correlated, which is the expected result. Also, relatively more

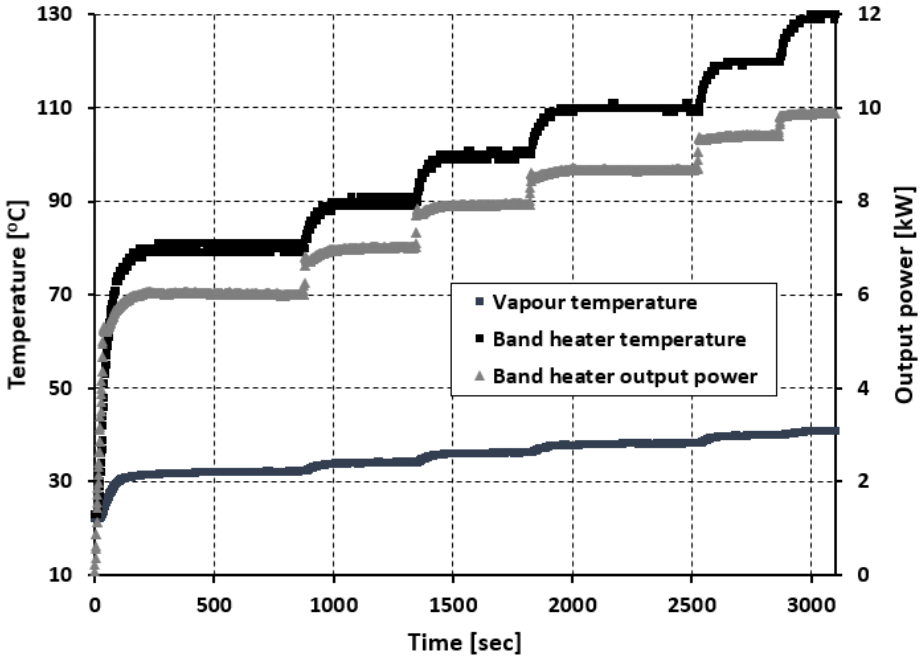


Figure 3.7: Performance of all band heaters after thermal paste is applied.

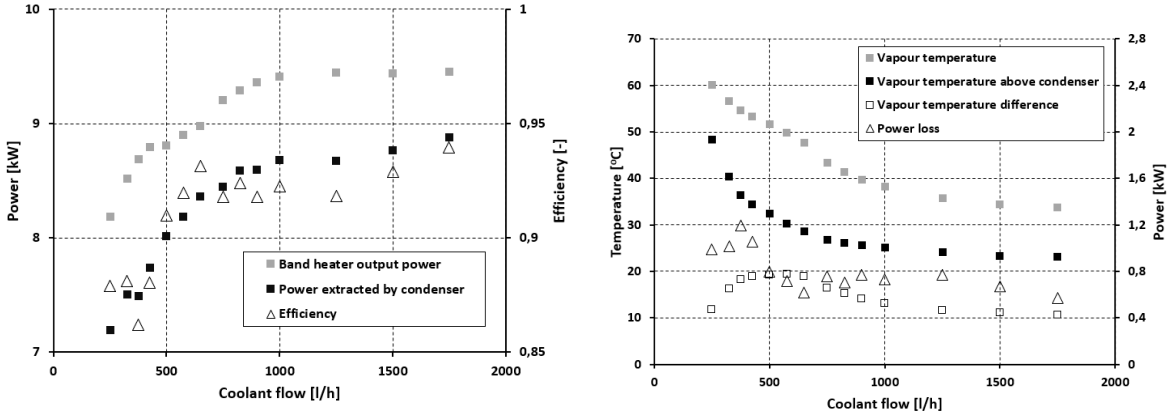


(a) In- and outgoing power (boxes) and the efficiency (triangles)

(b) Vapour temperature below and above the condenser (boxes) and the power loss (triangles)

Figure 3.8: Results of a test run without thermal insulation.

power gets into the condenser for higher coolant flows (indicated by the increasing efficiency). This is related to the fact that the vapour temperature is lower and thus a lower loss through the pipe wall. The vapour temperature for the given coolant flows is displayed in figure 3.8b. From the figure it becomes clear that the losses indeed become smaller for higher coolant flows. These results are similar to the results found by Zijm [27]. In figure 3.8b one can also see that the temperature above the condenser is significantly lower than the temperature below the condenser. This either means that the vapour has cooled down considerably before it reaches the top, or that there is an air pocket above the condenser that obstructs the vapour from coming to the top of the condenser. Just like the vapour temperature seems to go to an asymptotic value, the power loss also goes to its asymptote. This value is the power loss due to the high temperature of the band heaters. This is our base loss, because the temperature of the band heaters is fixed.

### 3.3.1. Verification

To verify if the numbers obtained make any sense, we will now estimate the thermal losses through the pipe wall. To simplify the problem, the top and bottom surface of the pipe is neglected. There is a small section above the condenser section, this is neglected as well. Also, the condenser section has been insulated in order to eliminate a temperature gain between the in- and outgoing coolant. It is therefore assumed that there will be no thermal losses through the outside wall of the condenser. What is left, is a section of roughly 6 meters with two glass sections of 1.5 meters each and 3 meters of copper tube

The first step is to estimate the thermal losses from the band heaters. We estimate the convective heat transfer coefficient to be 5 W/m$^2$K. The radiative heat transfer coefficient can be estimated using the following linearization:

$$h_r = 4\epsilon\sigma T_w^3 \tag{3.1}$$

Where $\epsilon$ is the emissivity of the steel band heater sheath, $\sigma$ the Stefan Boltzmann constant and $T_w$ the temperature of the wall. For the emissivity of steel we take 0.25. From figure 3.5 it became clear that the temperature of the band heaters is not uniform. To still put a number on the wall temperature, 120 $^o$C is taken. We must keep in mind that this is an underestimation. The radiative heat transfer coefficient is about 3.4 W/m$^2$K. The total heat loss from the band heaters then becomes:

$$\dot{Q} = (h_r + h_c) A_{bh} (T_w - T_e) \tag{3.2}$$

Where $h_c$ is the convective heat transfer coefficient, $A_{bh}$ is the outside band heater area and $T_e$ is the temperature of the environment. Filling in the numbers as given above, gives a loss off 70 Watts from the band heaters. To this loss, we must add the loss through the pipe wall in the adiabatic section.

To this end, we consider 3 meters of glass and 3 meters of copper and calculate the thermal losses through these sections. Since copper is a good thermal conductor, the thermal resistance across the wall is neglected. For glass, the the thermal conductivity is 1.2 W/mK [4] and it is not neglected. For both the glass and the copper the convective heat transfer coefficient is assumed to be 5 W/m$^2$K. The emissivity coefficients are 0.9 and 0.05 for glass and copper respectively. To calculate the loss through the copper wall, we can simply use formula 3.2. For the loss through the glass wall we take the wall resistance into account, hence we use the following formula:

$$\dot{Q} = U * (T_v - T_e) \tag{3.3}$$

Where U is defined as:

$$\frac{1}{U} = \frac{1}{(h_r + h_c) A_g} + \frac{1}{z_2}$$

Where $z_2$ is given by formula 2.19 and represents the resistance across the wall.

From figure 3.8b it becomes clear that we have to calculate the losses for different vapour temperatures. Because this is just an order of magnitude estimation, we calculate the losses for a vapour temperature of 60 $^o$C and 35 $^o$C, to see if the losses shown in figure 3.8b can be justified.

### 3.3.2. Losses through the copper section

Since we neglect the thermal resistance of the copper pipe, we can simply say that the wall temperature is equal to the vapour temperature. To calculate the losses through the wall, we use equation 3.2. Where $h_r$ is calculated using 3.1. For 35 $^o$C this thermal loss is equal to 40 Watt. For 60 $^o$C this loss is equal to 110 Watt.

### 3.3.3. Losses through the glass section

The resistance across the glass wall is by approximation constant in the temperature range mentioned above. Filling in the numbers we obtained into equation 2.19 gives $z_2$ to be $4.3 \bullet 10^{-3}$. We now calculate the radiative heat transfer coefficient using equation 3.1, this gives 6 W/m$^2$K and 7.5 W/m$^2$K for 35 $^o$C and 60 $^o$C respectively. We now can fill in formula 3.3, which gives 82 W and 248 W for 35 $^o$C and 60 $^o$C respectively.

Adding up the losses from the band heaters and the losses through the pipe walls, we get a heat loss of approximately 200 Watt if vapour temperature is 35 $^o$C. For 60 $^o$C the sum of all the losses is 430 Watt. From these numbers one can see that for the higher vapour temperatures, the losses are a factor 2 greater than for the lower vapour temperatures. This can also be seen in figure 3.8b. The losses that are calculated differ from the results obtained, but are still in the same order of magnitude. The error is probably due to a wrong estimation of the convective heat transfer coefficient. The author put it at 5 W/m$^2$K as a common value for free convection in still air, but since the laboratory is quite drafty, it might as well be 10 W/m$^2$K or higher. The estimations of the heat losses show a similar trend as can be seen in figure 3.8b. Hence, a recommendation would be to insulate the setup to lower these losses.

## 3.4. Resistance verification

In chapter 2, we estimated the resistances across the condenser and the evaporator. To see if the numbers calculated were in the right order of magnitude, we will now plot the resistances across the evaporator and the condenser. The resistance can be expressed as:

$$z = \Delta T / \dot{Q} \tag{3.4}$$

One problem that we now encounter is what temperature difference to take for the condenser. In the end, we need to find an average resistance across the condenser. It is therefore decided to take the average temperature of the in- and outgoing coolant and subtract this number from the vapour temperature just below the condenser. This gives an average temperature difference over the condenser wall. Another problem is what temperature difference to take for the evaporator. Since the surface temperature of the evaporator wall is unknown, we can only use the thermocouple reading from the band heaters. Earlier in this chapter it was shown that the resistance across the band heaters is significant. However, it expected that the resistance across the band heater and the interfacial resistance are constant since the band heaters are kept at a constant temperature. Therefore the temperature difference taken is the thermocouple reading from the band heater and the vapour temperature in the heat pipe. The resistance that will be calculated is therefore greater than the true value (since it includes resistance across the band heater and from the band heater to the evaporator wall), but the trend that is shown should still be valid.

### 3.4.1. Condenser resistance

Figure 3.9a shows that the resistance across the condenser becomes smaller for higher coolant rates. This means that if more power is going through the heat pipe, the resistance across the condenser gets smaller. This can also be seen in figure 3.10: the higher coolant flow gives a smaller temperature difference for the in- and outlet. Also, the temperature of the coolant gets closer to vapour temperature in the heat pipe, which decreases the thermal resistance across the condenser wall. The theoretical result is calculated using a number of equations from the Heat Atlas [22]. Chapter G2 titled: 'Heat transfer in concentric annular and parallel

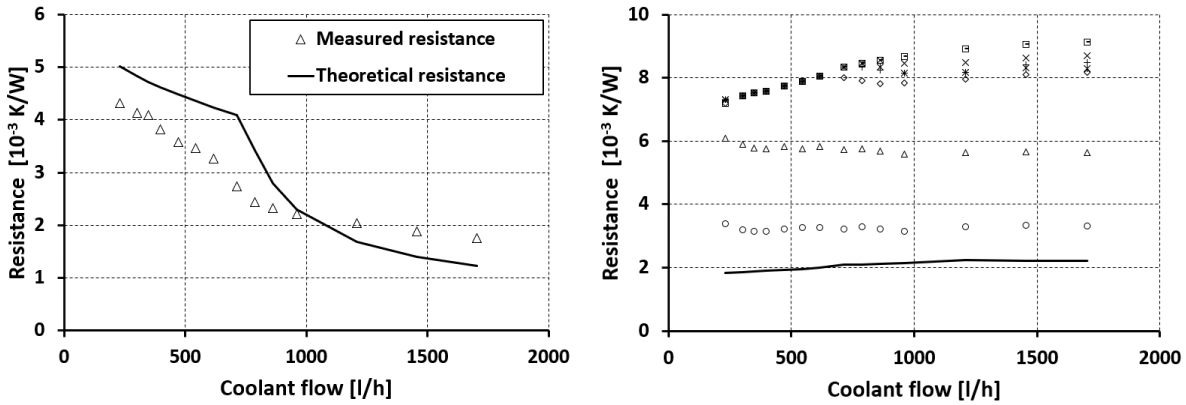


(a) Plot of the resistance of the condenser for a range of flow rates

(b) Plot of the resistance of the evaporator for a range of flow rates.

Figure 3.9: Resistance of the condenser (left figure) and the evaporator (right figure).

plate ducts', describes the equations that can be used to calculate the heat transfer coefficient for double walled pipes. The specific formulae used can be found in this chapter and will not be copied into this thesis. From these formulae a heat transfer coefficient can be isolated which is then converted to a thermal resistance. This thermal resistance gives a resistance from the condenser wall to the cooling water. The thermal resistance between the condenser wall and the vapour within the heat pipe is calculated using equation 2.24. The thermal resistance across the condenser wall is neglected. The thermal resistances obtained can be added to each other since the resistances are connected in series.

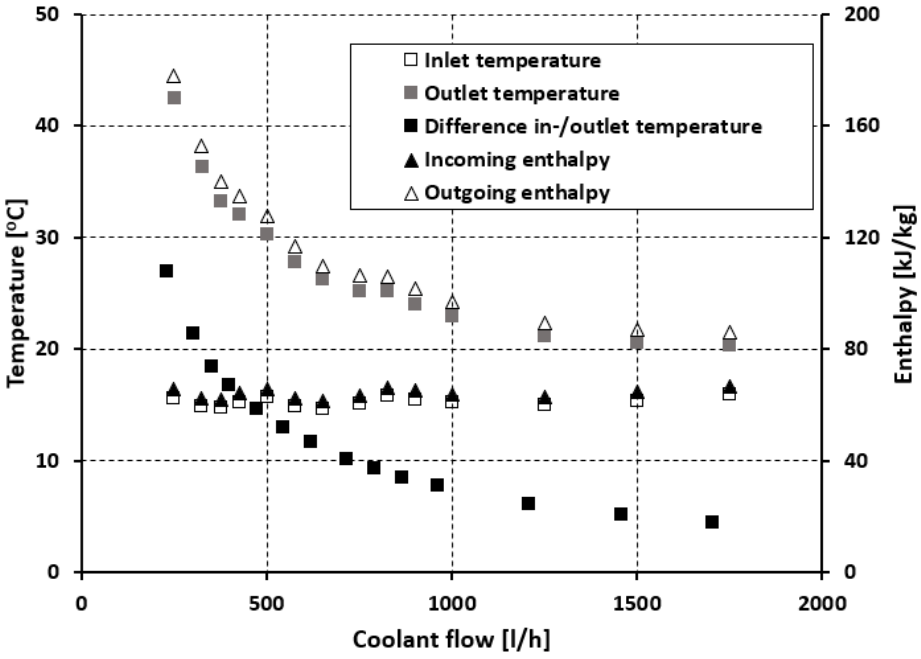


Figure 3.10: Plot of the temperature of the incoming and outgoing coolant from the condenser (boxes) and the enthalpy (triangles) of the coolant.

In figure 3.9a, one can see a sharp decrease in the theoretical thermal resistance around a coolant flow of 750 l/h. This is because the flow develops from a laminar flow regime into a transition regime. The decrease is not observed in the measured results. However, overall the measured results are in close accordance with the theoretical result. In paragraph 2.6.5, we found that the resistance across the condenser should be in the order of $1.8 \bullet 10^{-3}$ K/W. From figure 3.9a it becomes clear that number is only valid for high coolant flows. It should be noted that the change in resistance is dictated by the heat transfer from the condenser wall to the coolant. Not the resistance to get from the working fluid to the condenser wall, since this resistance is almost constant for all coolant flows. The thermal resistance from the condenser wall to the coolant is highly dependent on the coolant flow speed, as can be seen in formula 4.65 from Mills [15]. This explains the descending trend as shown in figure 3.9a.

The difference in the theoretical and measured thermal resistance has to do with the way the theoretical resistance is calculated. The calculation assumes that both the vapour temperature in the heat pipe and the coolant temperature are constant along the condenser wall. This gives an easier calculation process (since the physical properties of the coolant and condensing vapour do not vary), but the results are less accurate. The temperature of the vapour does vary, as can be seen in figure 3.8b, where the vapour temperature above the condenser is significantly lower than below the condenser. Also the temperature of the coolant is changing since it cools down the vapour in the heat pipe. One of the key numbers to determine the thermal resistance across the condenser wall is the Prandtl number. The Prandtl number for liquid water is highly dependent on the temperature of the water. For example, water at 20 $^{o}$C and at a pressure of 5 bar, has a Prandtl number of 6.9974, while at 50 $^{o}$C the Prandtl number is 3.5494 [17]. By averaging the temperature, variance in the Prandtl number and other properties are neglected, giving a less accurate result.

### 3.4.2. Evaporator resistance

In figure 3.9b one can see the theoretical thermal resistance from the evaporator wall to the liquid pool inside the heat pipe (the solid black line) and the measured thermal resistance. Since 8 different band heaters were used, 8 different temperatures are measured by the thermocouples that are placed on the band heaters. These 8 thermocouples all give a different thermal resistance. The two lowest measured resistances (indicated in figure 3.9b by the round markers and the triangles) is from two thermocouples that gave consistently lower temperature readings than the other thermocouples. Lower temperature measurements on the evaporator wall result in a lower resistance, as can be seen from equation 3.4. These low readings are there because the thermocouples have not been properly welded onto the sheath of the band heaters. If there is some air in between the thermocouple and the band heater wall, the thermocouple is thermally insulated from the band heaters and can therefore not give an accurate reading. The 6 other thermocouple readings all give a similar result. The difference in magnitude between the theoretical resistance and the measured resistance can be explained by the fact that theoretical resistance only accounts for the pool boiling resistance (equation 2.21), while the measured resistance also accounts for the interfacial resistance between the band heater and the evaporator wall, and the resistance across the band heater itself.

In chapter 2 the resistance across the evaporator wall was calculated. In paragraph 2.6.5 it was estimated that the resistance across the evaporator is $1.4 \bullet 10^{-2}$ K/W. This result was largely determined by the interfacial resistance between the evaporator wall and the band heaters. From figure 3.9b it becomes clear that this resistance is somewhat smaller, even when we include the resistance across the band heater itself. However, the value of 1000 W/m$^2$K as the interfacial conductance was an estimation, not a calculation. Both the theoretical result and the measured result have a similar upward trend. From equation 2.21:

$$z_{3,p} = \frac{1}{63(p_v/p_a)^{0.23} g^{0.2} \dot{Q}^{0.4} (\pi D_i l_e)^{0.6}}$$

it not obvious where this upward trend is coming from. In the denominator of this equation, the factor $\dot{Q}^{0.4}$ is shown. This would imply that for higher heat flows, the thermal resistance should go down. Figure 3.9b shows the opposite. However, since the vapour temperature rises considerably for low coolant flows (as can be seen in figure 3.8b), the saturation pressure in the heat pipe therefore rises as well (200 mbar at a coolant flow rate of 250 l/h and 65 mbar for 1500 l/h). This is a difference in pressure of a factor 3, while the heat flow only increases by a factor of 1.15. Since the decline in pressure is steeper than the increase of heat flow, the net result is an increase in the overall resistance.

# 4

# Conclusion

In chapter 2 we have seen an overview of the requirements that were taken into consideration for the design of the heat pipe. We have seen what limited the dimensions of the heat pipe, a motivation for the material choice and the expected limits for heat flow. Using two different methods we checked if the dimensions that were chosen would suffice to maintain a heat flow of 10 kW. After the initial calculations, the heat pipe was physically built and matched all requirements, except the heat flow of 10 kW. In chapter 3 we first encountered a disappointing total heat flow, but fixed this by applying contact thermal paste between evaporator wall and the electric heater. We saw that the temperature of the band heaters is far from uniform. There is a relatively large thermal resistance from the outside of the band heaters to the inside, as can be seen in figure 3.4. Even on the outside of the band heaters is a temperature profile visible. We saw also that the thermocouple was placed in a slightly cooler region of the band heater. If we sum all these factors up, we come to the conclusion that the temperature that is read from the thermocouple is unreliable. To fix this problem, a new thermocouple is recommended. A thermocouple that is placed in between the band heater and the evaporator wall. This way, one does not have to rely on the fickle measurements from the band heaters anymore. The thermocouple can for example be placed in a small, milled groove in the evaporator wall.

After the thermal paste was applied, the heat pipe started to perform as it was designed to do. After it was established that the heat pipe worked properly, the thermal losses were investigated for different coolant flow rates. To verify this result, the thermal losses were calculated for the two extreme vapour temperatures. These results showed that the thermal losses for the highest coolant flows should indeed be a factor 2 smaller than for the lowest coolant flows. The idea being, that at low coolant flows the vapour temperature rises, which will increase the thermal losses. This was confirmed by both the calculations and the experimental results.

## 4.1. Recommendations

The recommendation from the author would be to insulate the heat pipe, to decrease the thermal losses. A small investigation was made earlier on in the designing process and Rockwool shells were recommended in favour of Armaflex insulation. The shells are already available in the laboratory.

Another problem faced, was that the pump that should move the coolant from the hot side to the cold side, was not powerful enough to do so. It is recommended to replace the cooling water pump for a more powerful version so that temperature of the ingoing coolant can be controlled.

During the test to calculate the thermal losses of the heat pipe, a problem arose with the results. Especially at low coolant flows, the heat pipe seemed to be extremely efficient (around 100%). This result was not accordance with the expected outcome. After careful investigation, it became clear the flow meter was not properly callibrated. Especially at low flows, the flow meter was giving numbers that were too high. To combat this problem the author recommends to use multiple (properly calibrated) flow meters in parallel. So that the range at which the heat pipe can operate is extended and also the flow rate can be reliably measured.

The band heaters were calibrated during the construction of the setup. However, this was only done at full capacity. At this full capacity, the solid-state relay that controls the electricity, lets all of the 50 AC waves go through. At a lower capacity it only lets a certain portion of the waves through. The solid-state relay switches at a zero load. Hence the author and the electrical engineer assumed that the percentage of waves that is let through by the solid-state relay is a proper measure for the electric power that goes into the setup. However, it has not been checked if this is really the case. The test results seem to imply that it is, but it is not rigorously tested. The author would recommend to check if the percentage of electrical waves let through is indeed a proper measure for the in going electrical power.

The pressure sensor that was used during the project, have an accuracy of 0.6 mbar. Besides that this is not accurate enough, the pressure reading that it gave was unreliable. Sometimes it measured a pressure that was higher than the saturation pressure, sometimes lower. My recommendation is that the pressure sensor that is now used is replaced by a more accurate version.

### 4.1.1. Future work

A question that is not answered in this thesis is what the pressure losses are in the heat pipe. Given that the heat pipe is to be used for geothermal applications, what are the losses one has to consider while designing this heat pipe? More study has to be done into this subject. One consideration is that the speed at which the vapour flows in the heat pipe is highly dependent on the temperature of the vapour. Higher operating temperatures give a higher pressure and therefore increase the density of the vapour in the heat pipe. From equation 2.9 it can be seen that for higher density, the speed of the vapour decreases. Hence, the pressure losses are correlated with the vapour temperature in the heat pipe, but how they exactly interact, has to be further investigated.

Also, in this thesis, only the in going power and out going power were considered. It was measured that for higher heat flows, the efficiency of the heat pipe went up. But at these high coolant flows, the temperature of the outgoing coolant flow was much lower than for a low coolant flow. If one only considers the efficiency of how much power goes in versus how much heat comes out, one ignores if the heat is actually usable at that particular temperature. For example, the temperature of hot water in Dutch households is typically 60 $^{o}$C. If one wants to exploit geothermal sources to heat Dutch houses, the water temperature that goes into the homes is ideally around 60 $^{o}$C. A more in-depth study into exergy destruction must be done in order to calculate at which operating temperature a heat pipe truly performs optimally.

# A

# Appendix

## A.1. Technical drawings

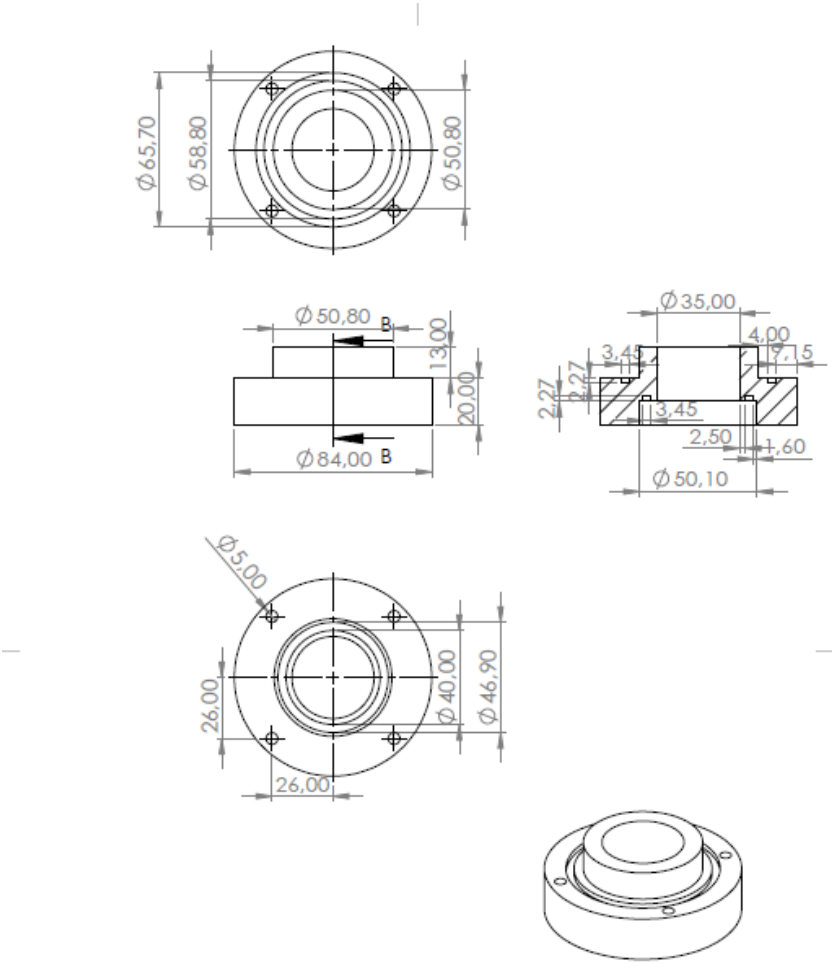


Figure A.1: Technical drawing of the glass holder mentioned in the second chapter

# Bibliography


[1] A. Acton. Heat pipes – performance of capillary-driven designs. Technical report, Engineering Sciences Data Unit, 1979.

[2] A. Acton. Heat pipes – general information on their use, operation and design. Technical report, Engineering Sciences Data Unit, 1980.

[3] A. Acton. Heat pipes – performance of two-phase closed thermosyphons. Technical report, Engineering Sciences Data Unit, 1983.

[4] M. Ashby. Granta design limited. CES Edupack, 2018. version 18.1.1.

[5] Shercliff H. Ashby, M. *Materials: engineering, science, processing and design*. Butterworth-Heinemann, Oxford, 2010.

[6] C. A. Busse. Theory of the ultimate heat transfer limit of cylindrical heat pipes. *International Journal of Heat and Mass Transfer*, 16(1):169–186, 1973.

[7] TC Direct. Single voeler knelkoppelingen. `https://www.tcdirect.nl/Default.aspx?level=2&department_id=294/1`, 2019. Accessed on 12-08-2019.

[8] EngineeringToolbox. Mineral wool insulation. `https://www.engineeringtoolbox.com/mineral-wool-insulation-k-values-d_815.html`, 2007. Accessed on 12-08-2019.

[9] R.S. Gaugler. Heat transfer device, 1942. US Patent 2350348A.

[10] KME Group. Sanco: eens en voor altijd. `https://www.kme.com/fileadmin/DOWNLOADCENTER/COPPER%20DIVISON/3%20Plumbing%20Tubes/1%20SANCO%C2%AE/SANCO_Product_Range_NL_2017.pdf`, 2017. Accessed on 09-05-2019.

[11] RKC Instruments Inc. Ma900/901. `https://docs.wixstatic.com/ugd/c114df_8d9f9f7f091b4612a0193b619a19cbe6.pdf`, 2001. Accessed on 27-08-2019.

[12] F. P. Incropera. *Introduction to heat transfer*. Wiley, New York, 1996.

[13] SpecView Corp & SpecView Ltd. Specview. `https://www.specview.com/`, 2019. Accessed on 27-08-2019.

[14] Milieudefensie. Olie- en gasportaal milieudefensie. `http://geo.solutions/olieengasportaal/`, 2019. Accessed on 09-08-2019.

[15] A. F. Mills. *Basic Heat and Mass Transfer*. Pearson, Harlow, Essex, 2004.

[16] H. Nguyen-Chi and M. Groll. Entrainment or flooding limit in a closed two-phase thermosyphon. *Journal of Heat Recovery Systems*, 1(4):275–286, 1981.

[17] National Institute of Standards and Technology. Reference fluid thermodynamic and transport properties. Refprop, 2010. Standard reference database 23, version 9.0.

[18] D. Reay. *Heat Pipes: Theory, Design and Applications*. Butterworth-Heinemann, Oxford, 2014.

[19] M. Shiraishi and S. Kikuchi. Investigation of heat transfer characteristics of a two-phase closed thermosyphon. *Journal of Heat Recovery Systems*, 1(4):287–297, 1981.

[20] S. D. Sriskandarajah. Thermophysical properties of heat pipe working fluids: operating range between –60 °c and 300 °c. Technical report, Engineering Sciences Data Unit, 1980.

[21] TNO. Aardwarmte. http://www.geologievannederland.nl/ondergrond/afzettingen-en-delfstoffen/aardwarmte, 2019. Accessed on 09-08-2019.

[22] Gesellschaft Verfahrenstechnik und Chemieingenieurwesen. *VDI Heat Atlas*. Springer Verlag, Heidelberg, 2010.

[23] Technische Unie. Flamco bsa tweedelige beugel. https://www.technischeunie.nl/product/prd1999901607, 2019. Accessed on 27-08-2019.

[24] Centraal Bureau voor de Statistiek. Energiebalans; aanbod, omzetting en verbruik. https://opendata.cbs.nl/statline/#/CBS/nl/dataset/83140NED, 2019. Accessed on 22-02-2019.

[25] Watlow. Mineral insulated (mi) band heaters. https://www.watlow.com/en/products/heaters/mineral-insulated-band-heaters, 2018. Accessed on 17-07-2019.

[26] C. Windenburg, D. F. Trilling. Collapse by instability of thin cylindrical shells under external pressure. *Transactions of the American Society of Mechanical Engineers*, 53(17a):819–825, 1931.

[27] P. Zijm. A geothermal heatpipe prototype, 2018. Master Thesis.